Dear Reviewer,

Thanks very much for your comments. We appreciate the time and effort taken to provide valuable comments on this manuscript. We have modified the manuscript accordingly. The changes in the manuscript are marked in red. Below are our responses:

Response to referee #1:

Major Comments

Comment_1: *Page 8, lines 185-187: the dispersion model accuracy significantly decreases in the case of too low and too high wind speeds. The upper wind speed has been fixed to 8m/s. How do the results depend on this value? Did you make sensitivity tests before fixing this value to 8m/s?*

Response:

Thanks very much for this comment. For high wind speed, or weak turbulence, the dispersion in the x direction is negligible in comparison with the advection (de Visscher, 2014). The dispersion model accuracy significantly decreases in the case of wind speeds < 1 m/s (de Visscher, 2014) and the critical wind speed is around 1.2 m/s. The high wind speeds may not affect the model accuracy, and we just limited our simulations to wind speeds < 8 m/s, because this range covers typical measurement conditions. We have revised the manuscript accordingly (lines 175-186). It is:

It should be noted that Briggs's equations are only suitable under the condition of x lower than 10 km. The dispersion in the wind direction is negligible in comparison with the advection when the wind speed is high, or for weak turbulence (de Visscher, 2014). In addition, the model accuracy significantly decreases in the case of wind speeds < 1 m/s (de Visscher, 2014). The critical wind speed for the Gaussian dispersion model is about 1.2m/s (de Visscher, 2014). For high wind speed, the effect of undetectable flux becomes very important (see e.g. results in Fig. 8). Thus for the general cases considered here measurements under high wind speed are not recommended. Only for very high emissions and close to the source (<1km), measurements for high wind speeds might be

meaningful, but such situations might be rare. Since our study focuses on the general cases, we limit it to wind speeds < 8m/s, because in the range up to 8m/s the general dependencies become obvious. Therefore, the wind speed range in our simulation is between 1.2 m/s and 8 m/s. The distance in our simulation is within 10 km.

Comment_2: *Page 9, lines 202-203: From where those reaction rate values come from? Literature source(s) should be added here.*

Response:

Thanks for this suggestion. The reaction rate values are from de Visscher, 2014. We have added this literature source accordingly.

Comment_3: *Page 12, lines 273-275: For low plume heights, the SCD could be assumed to be equal to the VCD. Did you determine from which plume height this assumption is not valid anymore?*

Response:

Thanks very much for this very important comment. We have investigated the dependence of the AMF on altitude via 3D RTM simulations. The results indicate that for a plume height around 250m, the AMF is typically between 1.05 and 1.3. The higher values are for high Aerosol load and high SZA (here only measurements below 75 ° are considered), the lower values are for low aerosol load and low SZA. That means that for our simulations, the VCDs are not exactly the same as the measured SCDs. However, the AMFs are still smaller than for measurements of horizontally extended plumes. For layer heights below 50m, the AMF is around 1.03 and the AMF error can be neglected. We therefore add the error of the AMF to the total error calculation and also add some discussions on AMF error (lines 344-354):

VCDs are derived from SCDs applying AMF. We calculated AMFs using the Monte Carlo atmospheric radiative transfer model McArtim (Deutschmann et al., 2011). For that purpose, we calculated 3-D box-AMF for different aerosol loads and solar zenith angle (SZA). It should be noted that the application of 3-D box-AMF (in contrast to 1-D box-AMF) is important for the measurements considered in our study, because horizontal extension of the plumes perpendicular to

the wind direction is rather short (compared to the average horizontal photon path lengths). Our simulations indicate that, for a plume height around 250m, the AMF is typically between 1.05 and 1.3. The higher values are for high Aerosol load and high SZA (here only measurements below 75° are considered), the lower values are for low aerosol load and low SZA. ±10%. For layer heights below 50m, the AMF is around 1.03 and the AMF error can be neglected.

We also added an error analysis on the AMF error from lines 646 to 667:

4.7 AMF error

AMF values depends on plume height, SZA and aerosol optical density (AOD) as shown in Figure 16. For plume heights < 50m, the AMF is around 1.03 and its error can be neglected. For plume heights ≦ 250m, the AMF error is about ±10%. Since the plume height in our study is about 250m, the contribution from the AMF error has to be taken into account.

Since VCDs are derived from SCDs by dividing the AMF, then AMF errors introduce VCD errors, which furthermore contribute to the emission flux errors. Wind speed uncertainty is the main error source when close to the source. With larger wind speed, the relative error of the wind speed becomes smaller which then also contributes less to the flux error. This indicates that the flux error that results from other error sources, such as the AMF error, have larger relative contributions under larger wind speed. Figure 17 presents R^2_{AMF} and the total relative errors for wind speeds of 1.2 m/s and 8 m/s. From Figure 17 we could see that R^2_{AMF} for SO_2 under the speed of 1.2 m/s is very small while it becomes larger at the speed of 8m/s, even near 0.5 when near the source. The NOx flux error, however, is less affected by the AMF error for $R^2_{AMF} < 0.1$.

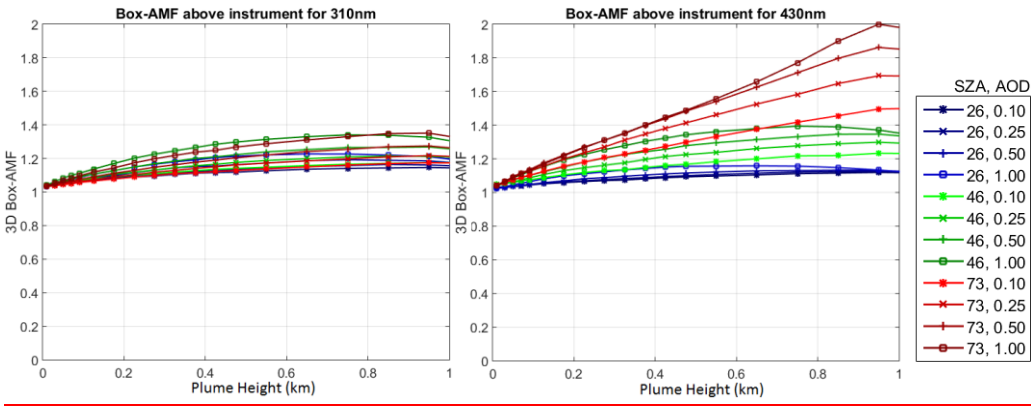

Figure 16. 3D Box-AMF dependence on plume height, SZA and aerosol optical density (AOD) for 310nm and 430nm. For the aerosols a box profile between the surface and 1km was assumed.

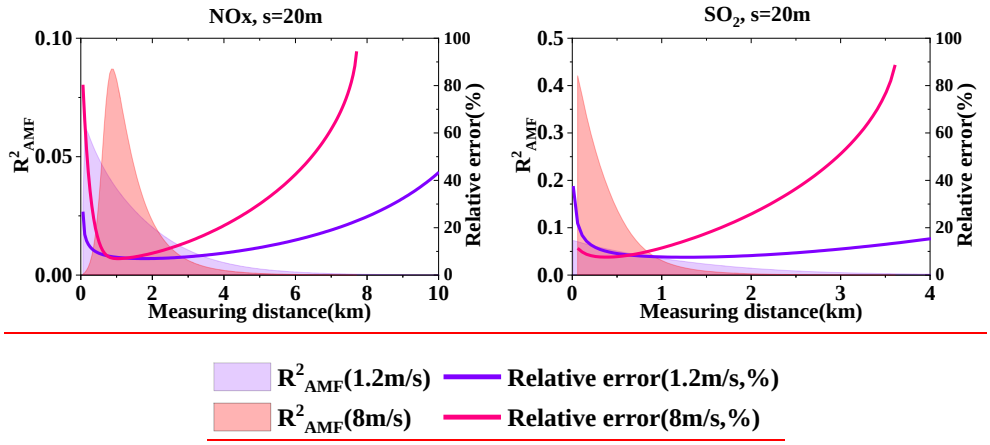

Figure 17. NOx and SO_2 total relative error, R^2_{AMF} of AMF error under different wind speed (Q = 100 g/s, s=20m).

Added Reference:

Deutschmann, T.; Beirle, S.; Frieß, U.; Grzegorski, M.; Kern, C.,Kritten, L.; Platt, U.; Pra-dos-Roman, C.; Pukite, J.; Wagner, T.; Werner, B.; Pfeilsticker, K., The Monte Carlo at-mospheric radiative transfer model McArtim: introduction and validation of Jacobians and 3-D features, J. Quant. Spectrosc. Ra., 2011, 112, 1119–1137.

Vandaele, A. C., Simon P. C., Guilmot, J. M. Carleer, M., Colin, R.: SO_2 absorption cross section measurement in the UV using a Fourier transform spectrometer, J. Geophys. Res., 99, D12, https://doi.org/10.1029/94JD02187, 1994.

Vandaele, A.C., Hermans, C., Simon, P.C., Carleer, M., Colin, R., Fally, S., Mérienne, M.F., Jenouvrier, A., Coquart, B.: Measurements of the NO_2 absorption cross-section from 42 000 cm−1 to 10000 cm−1 (238–1000 nm) at 220 K and 294 K, J. Quanr. .Specrrosc. Radior. Transfer, 59,171-184, DOI: 10.1016/S0022-4073(97)00168-4, 1998.

Comment_4: *Page 14, lines 308-309: Typical errors on NO_2 and SO_2 VCDs coming from previous studies are mentioned here and are used as is in the present work. These studies should be cited. Are the conditions assumed in those studies similar to the ones assumed by the authors, i.e. that SCD=~VCD and therefore the AMF error can be* neglected?

Response:

Thanks for this comment. We have cited those studies accordingly and please refer to our response to major comment_5. With respect to the AMF calculation and application, our study is partly different from previous studies. Some of previous studies measured more extended plumes, for which 'traditional' 1D-AMF calculations are appropriate. Since our study focusses on point source emissions, such 1D-simulations are not adequate. Instead, 3D-simulations taking into account the limited horizontal extent of the plume should be used. To our knowledge, such 3D-AMF simulations are applied for the first time in our study to point source emission measurements. In the revised version of the manuscript, we take the AMF value and AMF error into consideration. Please refer to our response to major comment_3.

Comment_5: *Page 15, Table 4: the detection limits for NO_2 and SO_2 SCDs are assumed to be two times the corresponding retrieval errors. This should be justified.*

Response:

Thanks for this comment. SCD retrieval errors are quantified by the fitting error (1σ error), and the mean detection limit is set to 2σ error (see e.g. Alicke et al., 2002,). We have revised the text accordingly (lines 333-343):

The SCD error can mainly be attributed to the DOAS fitting error of the SCD and the trace gas absorption cross-section error. Previous studies have indicated that the typical fit errors of NO_2 and SO_2 SCDs are $\pm(1\sim4)\times10^{15}$ molecules cm^{-2} and $\pm(1\sim6)\times10^{15}$ molecules cm^{-2}, respectively (Wagner et al., 2011; Wang et al., 2014; Wu et al., 2018; Davis et al., 2019). Thus in this study, we set the fit error of NO_2 and SO_2 to be $\pm2.5\times10^{15}$ molecules cm^{-2} and $\pm4\times10^{15}$ molecules cm^{-2} (1σ error), respectively. Here in addition, we use the 2σ values as detection limit (see e.g. Alicke et al., 2002; Platt and Stutz, 2008). The absorption cross-section errors are less than 3% for NO_2 and less than 2.4% for SO_2 (Vandaele et al., 1994, 1998). In this study, we set the total SCD error from gas absorption cross-section errors to 5% (Theys, et al., 2007) for both NO_2 and SO_2. Of course, these

values are only rough estimates, but they are useful to investigate the general dependencies of the total flux error.

Added Reference:

Alicke,B., Platt, U., Stutz, J.: Impact of nitrous acid photolysis on the total hydroxyl radical budget during the Limitation of Oxidant Production/Pianura Padana Produzione di Ozono study in Milan, J. Geophys. Res., 107, NO. D22, 8196, doi:10.1029/2000JD000075, 2002.

Davis, Z. Y. W., Baray, S., McLinden, C. A., Khanbabakhani, A., Fujs, W., Csukat, C., Debosz, J. and McLaren, R.: Estimation of NOx and SO_2 emissions from Sarnia, Ontario, using a mobile MAX-DOAS (Multi-AXis Differential Optical Absorption Spectroscopy) and a NOx analyzer, Atmos. Chem. Phys., 19, 13871–13889, https://doi.org/10.5194/acp-19-13871-2019, 2019.

Wang, T., Hendrick, F., Wang, P., Tang, G., Clémer, K., Yu,H., , Fayt C., Hermans, C., Gielen, C., Müller, J.-F., Pinardi, G.,Theys, N., Brenot, H., Roozendael, M. Van.: Evaluation of tropospheric SO2 retrieved from MAX-DOAS measurements in Xianghe, China, Atmos. Chem. Phys., 14, 11149–11164, doi:10.5194/acp-14-11149-2014, 2014.

Comment_6: *Pages 27-28, Section 4.6: If we want to use several scans to reduce the flux error, the elapsed time between two scans at the same distance from the source is then also an important parameter. I think this point should be at least briefly discussed here.*

Response:

Thanks for this comment. We have added a brief discussion at the beginning of section 4.8 (lines 670-677):

In our experiments, we only simulated a single scan of the plume by the mobile DOAS at each specific distance. In reality, we usually scan the plume cross-section several times in order to reduce the flux error. The elapsed time between two scans at the same distance from the source is then also an important parameter. The more of the elapsed time, the greater the uncertainties due to temporal variations of the flux and/or the wind fields are likely to be. Here, we assumed that the elapsed time is small and its influence can thus be neglected in our simulation. Figure 18 displays the simulation example of NOx and SO_2 flux error under different measurement times.

Technical corrections

Comment_1: *The abstract is much too long. Only the most relevant findings should be reported here.*

Response: Thanks for this suggestion. We have changed accordingly:

Mobile differential optical absorption spectroscopy (mobile DOAS) has become an important tool for the quantification of emission sources, including point sources (e.g., individual power plants) and area emitters (e.g., entire cities). In this study, we focused on the error budget of mobile DOAS measurements from point sources, and we also offered recommendations for the optimum settings of such measurements via a simulation with modified Gaussian plume model. Following the analysis, we conclude that: **(1)** The proper sampling resolution should be between 5 m and 50 m. **(2)** When measuring far from the source, undetectable flux (measured SCDs are under the detection limit) resulting by wind dispersion is the main error source. The threshold for the undetectable flux can be lowered by larger integration time. When measuring close to the source, low sampling frequency results in large errors and wind field uncertainty becomes the main error source of SO_2 flux (for NOx this error also increases, but other error sources dominate). More measurements times can lower the flux error that results from wind field uncertainty. The proper wind speed for mobile DOAS measurements is between 1 m/s and 4 m/s. **(3)** The remaining errors by [NOx]/[NO_2] ratio correction can be significant when measuring very close. To minimize the [NOx]/[NO_2] ratio correction error, we recommend minimum distances from the source, at which 5% of the NO_2 maximum reaction rate is reached and thus NOx steady-state can be assumed. **(4)** Our study suggests that emission rates < 30 g/s for NOx and < 50 g/s for SO_2 are not recommended for mobile DOAS measurements.

Based on the model simulations our study indicates that mobile DOAS measurements are a very well suited tool to quantify point source emissions. The results of our sensitivity studies are important to make optimum use of such measurements.

Comment_2: *Pages 3-4, lines 79-82: first letter of the first name should be removed in all the references that appear on these lines.*

Response: Thanks for this correction. We have removed the first letter of the first name accordingly.

Comment_3: *Figure 2: Point 4 in the list of dispersion simulation parameters: 'Disersion' -> 'Dispersion'*

Response: Thanks for this correction. We have revised the word.

Comment_4: *Page 7, line 164: Is there a reference for Pasquill and Gifford? If, yes it should be included in the list of reference.*

Response:

Thanks for this suggestion. The *Pasquill and Gifford* dispersion parameters calculated using Briggs's (1973) formulas are also from de Visscher, 2014. We have cited this reference accordingly.

Comment_5: *Page 8, line 186: maybe 'high' is preferable than 'strong'?*

Response: Thanks for this suggestion. We have changed the word 'high' in the manuscript accordingly.

Response to referee #2:

Major comments

Comment_1: *Two of the key error sources the authors discuss are wind direction and wind speed uncertainties. While I agree that wind speed introduces important uncertainties in flux estimates, I think that wind direction at such relatively short distance from a point source can be estimated with reasonable accuracy just from geometry. I strongly disagree with the way the authors have estimated wind uncertainties: They use a statistical evaluation of wind measurements at one site and interpret the standard deviations they find in these measurements as uncertainties which they then parametrise as a function of wind speed. However, this is not the quantity of interest for flux measurements, where wind speed and direction is usually taken from a close-by measurement or a model. I think either the authors need to explain why I am wrong, and this is after all a good representation of the uncertainty of the wind information usually employed in car-DOAS measurements, or they should use another, maybe simpler representation of the wind field uncertainty.*

Response:

Thanks for this suggestion. We agree that of course in general the use of nearby wind measurements would be preferred and errors related to wind field uncertainties should be calculated based on such wind measurements

However, the main aim of our study is to determine the error budget of the total flux and its different contributions in a general way. For that purpose, the parameterization of the wind speed uncertainty is very helpful to derive recommendations about favorable measurement conditions (e.g. wind speeds).

Therefore, we keep the results of the parameterization of wind field uncertainty.

Nevertheless, we agree that wind direction at such relatively short distance from a point source can be estimated with reasonable accuracy just from geometry. Thus the wind direction uncertainty contributes only a small error to the total flux error. We have re-simulated the results, and updated all

the results in the manuscript accordingly. We also added a brief discussion into section 2.6 (lines 299-302):

The wind direction uncertainties play a smaller role in point source flux measuring error (and can be derived from geometry), thus the uncertainties caused by the wind field are dominated by the wind speed uncertainties. The error term of the wind direction uncertainty is therefore removed.

Comment_2: *One important discussion point in the manuscript is the sampling error. Unfortunately, even after reading this part several times and checking the referenced papers for an explanation of what exactly this sampling uncertainty is, I was not able to understand it. In an ideal world, where the sky brightness does not change, the instrument has no dead time between measurements, and there are no nonlinear effects in the DOAS evaluation, the retrieved VCDs are the mean VCDs over the distance travelled during the integration time. If the wind field is homogeneous as I assume is the case in this study, then I fail to see where the "sampling error" comes into play. I think the authors need to provide a better explanation of what exactly they are referring to with this term.*

Response:

Thanks for this comment. The sampling resolution error results from the GPS measurement error and the sampling error. In general, GPS errors of neighboring flux contributions almost completely cancel each other. However, for the sampling error, we have added the explanation to the text (lines 389-393):

In actual measurements, if one distance is too long, and this happens to be inside the plume, while the next distance is too short but is already outside the plume, the flux will be overestimated in spite of the fact that the sum of the two distances has only a small error. In this case, the sampling error becomes important. The sampling error is largest when the sampling resolution is large. Thus a small and uniform sampling resolution is particularly important.

Comment_3: *One relevant point of the manuscript is the discussion of the NO_2/NOx ratio on the measurement uncertainty. Maybe I overlooked this information, but it was not clear to me how this uncertainty was computed – did the authors just assume that no correction is applied in the*

retrievals, so the error is defined as the difference between an assumed steady state ratio and the real NO_2/NOx ratio? Or is the uncertainty only increasing because the NO_2 column is decreasing as one approaches the stack? Please clarify in the manuscript.

Response:

Thanks for your comment.

We have added more information in section 4.4 (lines 539-552):

In actual measurements, especially for elevated point sources, the dependence of the [NOx]/[NO_2] ratio on the distance from the air parcels of the plume is difficult to measure. The [NOx]/[NO_2] ratio could e.g. be measured by an in situ instrument on the ground. However, in some cases the plume might not reach the ground. And even if it reaches the ground the measured [NOx]/[NO_2] ratio is probably not representative for the whole plume. Furthermore, also the ambient [O_3] could be measured, which would help to constrain the [NOx]/[NO_2] ratio. But also if O_3 measurements are available, the calculation of the [NOx]/[NO_2] ratio will have its uncertainties, and the derived [NOx]/[NO_2] ratio will again not be representative for the whole plume. Thus in our study, we calculate the [NOx]/[NO_2] ratio based on the dispersion model with some additional assumptions which are outlined in the text. In this way we can derive the general dependencies of the [NOx]/[NO_2] ratio on the plume distance and apply a corresponding correction. However, for the NOx flux calculations, even after the application of the [NOx]/[NO_2] ratio correction factor, substantial flux errors near the source might occur.

Comment_4: *I realize that this may be bordering onto a philosophical discussion, but I do not agree with the distinction the authors make between SCD uncertainty and undetectable SCD. In my view, this is two aspects of the same thing as the signal from the "undetectable SCD" is not missing, but just hidden in the noise. If the integration time is increased or more transects through the plume are averaged, then the "undetectable SCD" is reduced. The separation of these two effects may be illustrative to explain why measurements should not be done in the far field of the plume, but it is in my opinion not correct to claim that repeating measurements does not decrease the "undetectable SCD" as is stated in the manuscript. In general, I think that adding this as an*

additional error term is not mathematically correct.

Response:

Thanks for this suggestion. SCD retrieval error consists of a random and a systematic part. The random part mainly comes from the fit error (which tends to cancel out and has only a small contribution the flux error) and the systematic part mainly comes from the error of the trace gas absorption cross-section. The undetectable SCD is the SCD below the SCD detection limit and the detection limit can be estimated to be about 2 times the fit error (Platt and Stutz, 2008). Therefore, the SCD uncertainty mainly includes the undetectable SCD and the SCD error caused by the trace gas cross-section error. These two errors are independent from each other.

We have added a respective discussion on the error of the retrieved SCDs and (including the effects on the detectable flux and the gas absorption cross-section error) accordingly (lines 281-304):

The emission flux measurement errors by mobile DOAS have several sources: SCD fit errors, AMF errors, wind field uncertainties, and sampling resolution measurement errors (Johansson et al., 2008, 2009; Wagner et al., 2010; Ibrahim et al., 2010; Shaiganfar et al., 2011, 2017; Rivera, et al., 2012).

The uncertainty of the derived SCD from the DOAS fit has a random and systematic part. For the random part it can be assumed that in general it cancels out (in combination with the sampling resolution error it can have a very small contribution). Thus, its direct effect on the total flux error is neglected in the following. However, from the fit error also the detection limit is estimated. For SCDs below the mobile DOAS detection limit, undetectable SCDs result in undetectable flux and therefore the fit error indirectly contributes to the total flux error.

The systematic part of the SCD error caused by the uncertainty of the trace gas absorption cross-section is independent from the SCD fit error and is therefore included as an additional term in the total flux error calculation.

We assume that these errors are random, have a Gaussian distribution and are independent of each other. Then the total relative error of the emission flux is given by:

$$E_{total} = \frac{F_{err}}{D \cdot Q} \times 100\% = \frac{\sqrt{\Delta F_{cro}^2 + \Delta F_{uf}^2 + \Delta F_{AMF}^2 + \Delta F_{u}^2 + \Delta F_{s}^2}}{D \cdot Q} \times 100\% \quad (16)$$

where F_{err} is the flux error; ΔF_{cro} is the flux error introduced by gas cross-section error; ΔF_{uf} is the undetectable flux; ΔF_{AMF} is the flux error introduced by AMF errors; ΔF_u is the flux error introduced by wind speed uncertainty. The wind direction uncertainties play a smaller role in point source flux measuring error (and can be derived from geometry), thus the uncertainties caused by the wind field are dominated by the wind speed uncertainties. The error term of the wind direction uncertainty is therefore removed. ΔF_s is the emission flux error introduced by sampling resolution measurement error and it can be neglected (see section 4.1).

We have added discussions on the undetectable flux and gas absorption cross-section error accordingly:

4.5 Undetectable flux

As discussed in sections 4.3, undetectable flux dominates the flux error when far from source. In the following, we discuss further details of the undetectable flux error. The undetectable flux is caused by SCDs below the detection limit. Following Platt and Stutz (2008), we set the detection limit as 2 times the fit error. While the exact value of the detection limit might be different for different instruments and measurement conditions, we use this value to derive the general dependencies of this error term and its contribution to the total flux error.

VCDs are sensitive to wind speeds and the dispersion (Eqs. 9 and 10), so is the undetectable flux. We calculate the undetectable flux and its R_{uf}^2 along wind direction (equal to along the measuring distance) as shown in Figure 14 (for an emission rate of 100 g/s). As discussed, the main driver of undetectable flux increasing trend along the wind direction is attributed to the wind dispersion as can be seen from Figure 14. With measuring distance far away, the undetectable flux gradually dominates the flux error which can be denoted by R_{uf}^2 trend. Large wind speed also results in quick dispersion thus leads more undetectable flux. The R_{uf}^2 and the undetectable flux increases rapidly under the wind speed of 8 m/s than that of 1.2 m/s for both NOx and SO_2.

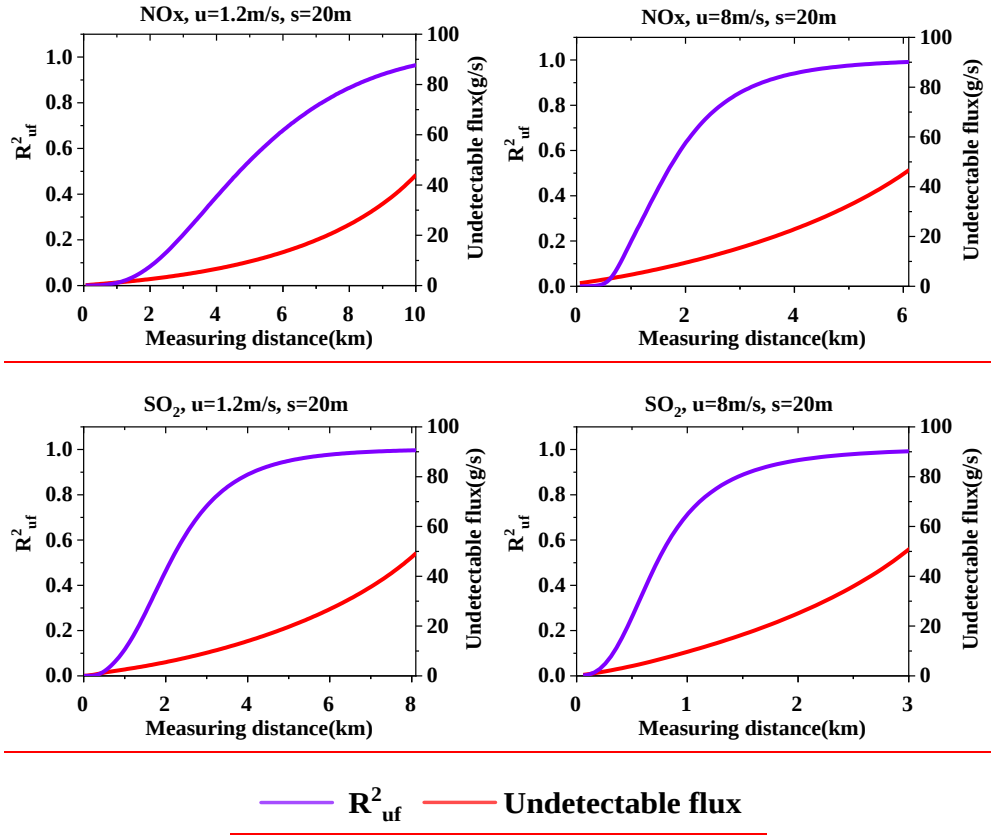

Figure 14. NOx and SO_2 absolute flux error, and the R^2_{uf} that SCD uncertainties resulting in (Q = 100 g/s)

4.6 Gas absorption cross-section error

As discussed in section 2.6, the gas absorption cross-section error contribution to SCD errors is independent of the SCD fit error. Uncertainties of the trace gas cross-sections cause systematic SCD uncertainty. We calculated R^2_{cro} along the wind direction and the total relative errors at the speed of 1.2m/s and 8m/s, as shown in Figure 15. The R^2_{cro} variation trend is similar to R^2_{uf} in section 4.6 due to the relative error variation. However, maximum R^2_{cro} has subtle difference but varies apparently along the wind direction under different wind speed, which indicates that R^2_{cro} is not very sensitive to wind speeds but sensitive to the dispersion. From Figure 15 we see that R^2_{cro} could approach 0.5, which means that gas cross-section error might even become the main error source. However, when R^2_{cro} is close to 0.5, the relative errors of NOx and SO_2 are at low levels. This further suggests the trace gas cross-section error has an overall small contribution to the total flux

error.

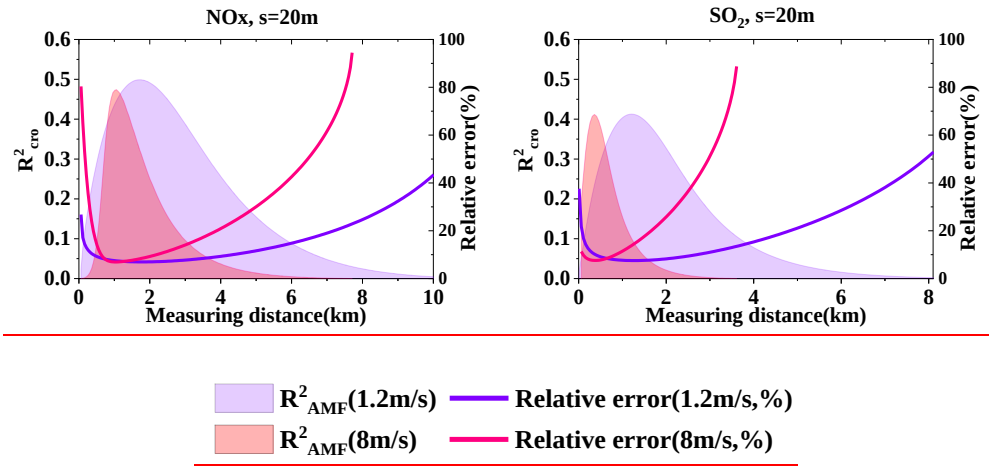

Figure 15. NOx and SO_2 R^2_{cro} of absorption cross-section error under different wind speed (Q = 100 g/s)

Comment_5: *The authors took a "top-down" approach for this manuscript, showing simulation results and then explaining them. While I understand that this is how science often works, it does not necessarily help in making the manuscript focused and revealing the underlying physical effects. In my opinion, a "bottom-up" approach explaining the key effects (such as dependence of VCD on wind speed, NOx/NO_2 ratio on time since emission, sampling error on measurement distance) and then illustrating it in the simulation results.*

Response:

Many thanks for this comment. This study aims to offer recommendations for the optimum settings of mobile DOAS measurements. Therefore, a universal and complete approach is very important. Nevertheless, we have added "*a 'bottom-up' approach explaining the key effects*" at the beginning of section 2.6(lines 270-280):

Emission flux measurements errors not only arise from measurement errors but also depend on other factors, such as wind speed, measuring distance, [NOx]/[NO_2] ratio and the sampling resolution.

Since the VCD is inversely proportional to the wind speed (Eqs.9 and 10), the higher the wind speed is, the lower the VCD. This means more measurements at the edge of plume would be under the detection limit at higher wind speeds causing more undetectable flux. The VCD is also inversely

proportional to measuring distance (Eqs.9 and 10). This means that the undetectable flux increase with measuring distance. Since the [NOx]/[NO_2] ratio depends on the measuring distance (see figure 10), a large [NOx]/[NO_2] ratio correction error occurs when the measuring distance is small. Finally, the sampling error can be reduced with improved sampling resolution.

Comment_6: *Overall, the manuscript would benefit from detailed proof reading. In some parts, in particular the description of the plume modelling, it is difficult to follow because of the use of English. In response to a suggestion from the quick-look review, the authors have in part introduced "air parcel" where they used "plume" before, but that did unfortunately not help to clarify this section. I hope that this section can be made clearer. Also, the use of "ambient SCD" is confusing and should be replaced by another formulation, maybe simply SCD.*

Response:

Thanks for the suggestion and we have revised the manuscript accordingly. We have introduced air parcel in many other places, and also substituted "SCD" for "ambient SCD".

To introduce the air parcel, we have also added at the following text at the beginning of section 2.1 (lines 107-109):

(2) The plume is diluted by the wind along the wind direction (*x* axis). The random movement of air parcels dilute the plume also in the cross-section and in the vertical directions (*y* axis and *z* axis).

We also tried to improve the use of the English language.

Detailed comments

Comment_1: *Abstract: Too long, please just summarize the main points instead of giving a detailed account of the study.*

Response: We have changed accordingly and it is:

Mobile differential optical absorption spectroscopy (mobile DOAS) has become an important tool for the quantification of emission sources, including point sources (e.g., individual power plants) and area emitters (e.g., entire cities). In this study, we focused on the error budget of mobile DOAS

measurements from point sources, and we also offered recommendations for the optimum settings of such measurements via a simulation with modified Gaussian plume model. Following the analysis, we conclude that: **(1)** The proper sampling resolution should be between 5 m and 50 m. **(2)** When measuring far from the source, undetectable flux (measured SCDs are under the detection limit) resulting by wind dispersion is the main error source. The threshold for the undetectable flux can be lowered by larger integration time. When measuring close to the source, low sampling frequency results in large errors and wind field uncertainty becomes the main error source of SO_2 flux (for NOx this error also increases, but other error sources dominate). More measurements times can lower the flux error that results from wind field uncertainty. The proper wind speed for mobile DOAS measurements is between 1 m/s and 4 m/s. **(3)** The remaining errors by [NOx]/[NO_2] ratio correction can be significant when measuring very close. To minimize the [NOx]/[NO_2] ratio correction error, we recommend minimum distances from the source, at which 5% of the NO_2 maximum reaction rate is reached and thus NOx steady-state can be assumed. **(4)** Our study suggests that emission rates < 30 g/s for NOx and < 50 g/s for SO_2 are not recommended for mobile DOAS measurements.

Based on the model simulations our study indicates that mobile DOAS measurements are a very well suited tool to quantify point source emissions. The results of our sensitivity studies are important to make optimum use of such measurements.

Comment_2: *Somewhere you should have a brief discussion of those aspects of the measurements which also lead to errors, but are not treated in this study, for example stratospheric correction, uncertainty in background measurement, non-Gaussian behavior of plume, vertical wind shear, …*

Response:

Thanks for this suggestion. We have added a brief discussion into the section 4.10.3 (lines 837-843):

The Gaussian dispersion model was assumed in the forward model during our discussion of the emission flux error budget. The dispersion in actual measurements, however, depends on meteorological conditions and surrounding terrain. Also a non-Gaussian behavior of the plume and vertical wind shear might contribute to the total flux error. Thus, the results of this study should be

seen as a lower limit of the total flux errors. In some cases, for NO_2, also the stratospheric absorption might become important. However, this might only happen for very long measurement durations or for measurements at high SZA.

Comment_3: *Section 2: I think it would be good to have a brief description of flux derivation with car-DOAS measurements first to remind all readers of how this is done and what the relevant quantities are. Later in this section, one could then refer to this introduction.*

Response:

We have moved some parts from section 2.5 to the beginning of section 2.1(lines 93-100):

The NOx and SO_2 emission flux of the point source can be well measured by the mobile DOAS. The equation for calculating the emission flux in the discrete form is expressed as

$$F = \sum_j VCD_j \cdot \vec{u}_j \cdot \vec{n}_j \cdot s_j \quad (1)$$

where F is the emission flux; $VCD_j = SCD_j / AMF_j$, SCD_j is the SCD for mobile DOAS measurements along the measurement route; AMF_j is the Air Mass Factor; $\vec{u}_j$ is the wind field; $\vec{n}_j$ is the vector pointing to the right of the driving direction and parallel to the Earth's surface; and s_j is the sampling resolution. For an isolated point source, the mobile DOAS can measure underneath the plume in downwind direction to quantify the emission flux.

Comment_4: *Section 2.1: The wording here is in parts confusing – "emission flux simulation" should be "simulation of emission flux measurement" as it is not the emission flux itself which is simulated.*

Response:

We have changed it to "simulation of emission flux measurement" and also in figure 2.

Comment_5: *Table 2: I'd suggest to remove those cases which are not use in this work (D, E, F)*

Response: We agree. We have removed these cases.

Comment_6: *Lines 175 – 183: I'm confused by this part which suggests that some temporal variations of the wind field need to be taken into account. However, as far as I understand the simulations, this is not the case. Please clarify and if this is not used in the simulations, please remove it.*

Response: We agree. We have removed it.

Comment_7: *Section 2.2.2: Please re-read carefully and make clear where you talk about the whole plume, a transect of the plume or an air parcel within the plume. For example, in line 200 you write "[O_3] is the mean concentration in the plume at time t" but in a static model as I assume you have, there are no changes with time. I assume in this case you are talking about the [O_3] in an individual air parcel moving through the plume. In line 208, you write "For simplicity, we assumed that the O_3 concentration within the air parcel of the plume is the same everywhere", but I assume that you mean that [O_3] is the same on a transect of the plume.*

Response:

Thanks for this correction. We have moved the sentences (original lines 206-209) here and revised accordingly (lines 205- 209):

where [gas] stands for the concentration of a particular gas; $[O_3]_t$ is the O_3 concentration in the air parcels of the plume at time *t; t* is the time period after NOx is emitted into the atmosphere. We assumed that at the beginning there is no O_3 in the air parcels of the plume. During the mixing with outside air, the O_3 concentration within the air parcels increases. For simplicity, we assumed that the O_3 concentration is the same everywhere in a transect of the plume.

Comment_8: *Section 2.2.2: In my opinion, additional assumptions were made in this section which should be mentioned, in particular that no NOx is present in ambient air as otherwise this would be mixed into the plume and more importantly, that no O_3 is consumed in the reaction with NO (which is clearly not correct). Please add this to the discussion.*

Response:

Thanks for this advice. We have added the following text to the discussion into subsection 2.2.2

(lines 190-197):

In this study, we did not take Volatile Organic Compounds (VOCs) into consideration; thus, a NOx balance would not be broken. Moreover, we assume that no NOx is presented in the ambient air and no O_3 is consumed in the reaction with NO. In most cases, both assumptions are reasonable, especially as long as the background NOx concentration has no strong spatial-temporal variation. However, for very high emission rates, the assumption that no O_3 is consumed in the reaction with NO might be violated (a simple criterion to identify such cases might be to check whether the NOx mixing ratios are higher than the ambient O_3 mixing ratios). If this is the case, the conversion of NO to NO_2 will be delayed.

Comment_9: *Equation 12: I think it would be good to explicitly show the dependence of* R_{NOx} *on (x) here.*

Response:

Thank you for advice. We have added a sentence to explicitly show the dependence of R_{NOx} on (x) (lines 243-245) and it is:

Since NOx disperses along the wind direction and R_{NOx} is a function of *t*, this means that R_{NOx} also varies with distance. The detailed relationship between the distance and R_{NOx} will be discussed in subsection 4.4.

Comment_10: *Equation 13: Please introduce* $\triangle F$ *and l. Do you assume that there is no NO2 or SO2 outside the plume?*

Response:

We have introduced $\triangle F$ *and l* accordingly (lines 251-252):

ΔF_j is the flux along the measurement route *l* in theory. For mobile DOAS measurements, ΔF_j should be given by Eq. (13).

We assumed that there is no NO_2 or SO_2 outside the plume and we have modified the assumption (3) in section 2.2 (lines 110-112):

(3) The topography around the point source is flat and the background concentration of the pollutants is regarded as zero. In case of non-negligible background concentrations, the VCDs in the plume have to be calculated as difference to the background.

Comment_11: *Equation 14: For clarity, $\triangle F$ and s should also have an index j here.*

Response:

Thanks for this suggestion. We have added the index *j to* $\triangle F$ and *s*.

Comment_12: *Equation 16: Why do you change notation here for the inner product? Why is the index now i and no longer j ?*

Response:

Thanks for this comment. We have unified the indexes as *j* from these equations.

Comment_13: *Equation 18: In order to be able to write the total error in this way, you need to assume that the errors are random, have a Gaussian distribution and are independent of each other. Is that a reasonable assumption?*

Response:

Thanks for this advice. It is a reasonable assumption and we have added this assumption before this equation (lines 294-295, please also refer to the response to major Comment_4).

Comment_14: *Equation 18: Why is Q used here instead of F ?*

Response:

For a plume cross section at a given distance, the flux (*DQ* in Equation 18) includes the detectable flux (*F*) and the undetectable flux($\triangle F_{uf}$) in theory. When the measuring distance is close to the source, $DQ \approx F$. However, this is not true when far from the source. Therefore, using *DQ* here is more reasonable and reprensentive, and this also ensures the consistency of the error evaluation criteria.

Comment_15: *Line 310: I agree that GPS errors tend to cancel, but this is not necessarily true for flux errors. If one distance is too long, and this happens to be inside the plume, while the next distance is too short but is already outside the plume, the flux will be overestimated in spite of the fact that the sum of the two distances has only a small error.*

Response:

Thanks for this comment and we agree. This is the sampling error. This scenario can indeed become important in actual measurements. In this case, a relatively small and uniform sampling resolution is particularly important. That is another reason that we only recommended the sampling resolution 5~50m, and this recommendation is also to minimize a potential flux overestimation. We have added a brief discussion of this scenario into the section. (lines 389-393):

In actual measurements, if one distance is too long, and this happens to be inside the plume, while the next distance is too short but is already outside the plume, the flux will be overestimated in spite of the fact that the sum of the two distances has only a small error. In this case, the sampling error becomes important. The sampling error is largest when the sampling resolution is large. Thus a small and uniform sampling resolution is particularly important.

Comment_16: *Section 4.3.1.1: There is also the effect of the plume width decreasing with increasing wind speed which counteracts the effect of increasing "undetectable SCD".*

Response:

We agree. The plume width we referred here is the width that can be detected by mobile DOAS. As the SCD is inversely proportional to the wind speed, this results in lower SCD under large wind speed and the "detectable SCD" decreases.

Comment_17: *Line 498: I understand the idea of the authors that if NOx is in steady state, it is easy to compute the NO_2/NOx ratio. However, at least in principle, one can estimate the NO_2/NOx ratio from the ambient O_3 concentration, the wind speed and the distance from the source as explained earlier in the manuscript.*

Response:

We agree that one can estimate the NO_2/NOx ratio from the ambient O_3 concentration in principle. In actual measurement, it is hard to estimate the NO_2/NOx ratio along the distance from the ambient O_3 concentration, the wind speed and the distance, although it is easy to realize in the simulation.

Comment_18: *Line 542: I don't think that this estimate is really conservative as two assumption son the NO to NO_2 conversion were made which both go into the direction of too fast conversion: 1) instantaneous mixing of O_3 into the plume and 2) no consumption of O_3 in the reaction with NO. In reality, the center of the plume will have lower O_3 than the outer parts and O_3 levels will be generally lower than in the ambient because of the high NO concentration inside the plume.*

Response:

We agree that and we have removed this discussion accordingly.

Comment_19: *Line 554 and following: It is still not clear to me why the absolute retrieval error decreases at large distance. This is counterintuitive to me.*

Response:

Thanks for this comment. The retrieval error here we referred is the DOAS fit error (we have revised 'retrieval error' as 'fit error' in the manuscript). When at larger distance, the flux error caused by SCD fit error decreases. We have removed section 4.5 (original title: **4.5 Retrieval error**) and please refer to the response to major comment_4.

Comment_20: *Figure 14: I do not understand why absolute flux retrieval errors are shown here – relative errors (not R2 but relative errors of the total flux) would be easier to understand.*

Response:

Thanks for this comment. We have removed section 4.5 (original title: **4.5 Retrieval error**). Please refer to the response to detailed comment_19.

Comment_21: *Line 574: As discussed above, I disagree with the statement that the undetectable flux cannot be reduced by multiple measurements.*

Response:

We agree that the undetectable flux can be reduced by multiple measurements. However, in reality this is often not possible because it requires that all measurement conditions (e.g. the wind field or the background concentrations) stay unchanged. This means that the undetectable flux is hard to be lowered by more time scanning in the actual measurements, although it can be easily realized in theory. Therefore, we regard the undetectable flux as the second error source, and in reality, it is difficult to reduce it by multiple measurements. We have added the following discussion on this to the text (lines 678-688):

The error sources of the emission flux can be classified into 2 types. The first is the measurable error/uncertainty: wind speed uncertainty, AMF error and undetectable flux. The second is: [NOx]/[NO_2] ratio correction error near the source and the gas absorption cross-section error. The flux error resulting from the first type of error source can be lowered by scanning the plume more times while the second cannot. Undetectable SCDs result in undetectable flux, and it can be reduced by more measurements times in theory. In reality, this is often not possible because it requires that all measurement conditions (e.g. the wind field or the background concentrations) stay unchanged. This means that the undetectable flux is hard to be lowered by more time scanning in the actual measurements, although it can be easily realized in theory. Therefore, in practice also the undetectable flux error belongs to the second type of errors, which cannot be reduced by multiple measurements.

Comment_22: *Figure 19: As Figure 14 – why absolute instead of relative flux errors?*

Response:

Absolute flux errors could help to understand the main driver of the total flux errors. The causes of the total relative error differences at a prescribed sampling resolution have been analyzed in subsection 4.9.1 (the original is 4.7.1) and it is not necessary to show absolute flux error again. We have therefore removed the absolute relative flux errors and revised the analysis accordingly.

Comment_23: *Line 701: Why do lower emission rates lead to variations in plume width? In relative units, this should not be the case.*

Response:

The plume width in this manuscript is referring to the width that mobile DOAS could detect. Lower emission rates lead to lower VCDs and to more measurements at edge of the plume below the detection limit. Thus, "lower emission rates lead to a reduction of the measurable plume width".

We have clarified the plume width (lines 806-808):

From Eqs. (9), (10), and (11) we know that the VCD(x,y) is proportional to the emission rate, which means that lower emission rates generate lower VCD(x,y), leading to a reduction of the measurable plume width with SCDs above the detection limit.

Comment_24: *Line 787: Which missing error source are you referring to?*

Response:

Thanks for this comment. The "missing error source" is not a good expression in the manuscript but we missed revising it during the revision process. We have removed it.

Thank you for taking care of our manuscript.

Kind regards,

Yeyuan Huang, on behalf of all authors.

The quantification of NOx and SO_2 point source emission flux errors of mobile DOAS on the basis of the Gaussian dispersion model: A simulation study

Yeyuan Huang[1,2], Ang Li[1], Thomas Wagner[4], Yang Wang[4], Zhaokun Hu[1], Pinhua Xie[1,2,3], Jin Xu[1], Hongmei Ren[1,2], Julia Remmers[4], Xiaoyi Fang[5], Bing Dang[6]

[1]Key Laboratory of Environmental Optics and Technology, Anhui Institute of Optics and Fine Mechanics, Hefei Institutes of Physical Science, Chinese Academy of Sciences, Hefei, 230031, China.

[2]University of Science and Technology of China, Hefei, 230026, China.

[3]CAS Center for Excellence in Regional Atmospheric Environment, Institute of Urban Environment, Chinese Academy of Sciences, Xiamen, 361000, China.

[4]Max Planck Institute for Chemistry, Mainz, Germany.

[5]Chinese Academy of Meteorological Science, Beijing, 100081, China.

[6]Beijing Municipal Climate Center, Beijing, 100089, China.

Correspondence to: Ang Li (angli@aiofm.ac.cn), Pinhua Xie (phxie@aiofm.ac.cn) and Yang Wang(y.wang@mpic.de)

Abstract: Mobile differential optical absorption spectroscopy (mobile DOAS) has become an important tool for the quantification of emission sources, including point sources (e.g., individual power plants) and area emitters (e.g., entire cities). In this study, we focused on the error budget of mobile DOAS measurements from point sources, and we also offered recommendations for the optimum settings of such measurements via a simulation with modified Gaussian plume model. Following the analysis, we conclude that: **(1)** The proper sampling resolution should be between 5 m and 50 m. **(2)** When measuring far from the source, undetectable flux (measured SCDs are under the detection limit) resulting by wind dispersion is the main error source. The threshold for the undetectable flux can be lowered by larger inte-

gration time. When measuring close to the source, low sampling frequency results in large errors and wind field uncertainty becomes the main error source of SO_2 flux (for NOx this error also increases, but other error sources dominate). More measurements times can lower the flux error that results from wind field uncertainty. The proper wind speed for mobile DOAS measurements is between 1 m/s and 4 m/s. **(3)** The remaining errors by [NOx]/[NO_2] ratio correction can be significant when measuring very close. To minimize the [NOx]/[NO_2] ratio correction error, we recommend minimum distances from the source, at which 5% of the NO_2 maximum reaction rate is reached and thus NOx steady-state can be assumed. **(4)** Our study suggests that emission rates < 30 g/s for NOx and < 50 g/s for SO_2 are not recommended for mobile DOAS measurements.

Based on the model simulations our study indicates that mobile DOAS measurements are a very well suited tool to quantify point source emissions. The results of our sensitivity studies are important to make optimum use of such measurements.

1 Introduction

Nitrogen oxides (NOx = NO + NO_2) and sulphur dioxide (SO_2), poisonous and harmful trace gases in the atmosphere, are critical participants in tropospheric chemical reactions (Seinfeld and Pandis, 1998; Beirle et al., 2003). NOx and SO_2 are emitted into the atmosphere via natural and anthropogenic emissions, especially from traffic and industries. In recent years, China has experienced large areas of haze pollution, which have drawn worldwide scrutiny due to their NOx, SO_2, and volatile organic compounds content, although strict policies designed to control the emission of pollution gases have been implemented (Richter, et al., 2005; Ding et al., 2015; Jin et al., 2016; Zhang et al., 2019, 2020). It is of great significance to study gas emission pollution both qualitatively and quantitatively.

Differential Optical Absorption Spectroscopy (DOAS) is a technique developed in the 1970s that focuses on the telemetering of atmospheric gases, particularly trace gases (Platt and Stutz, 2008). After years of research, various types of DOAS technology have been comprehensively developed, including LP-DOAS, MAX-DOAS, and mobile DOAS.

Mobile DOAS technology was originally used to measure volcanic SO_2 emissions (Bobrowski et al., 2003; Edmonds et al., 2003; Galle et al., 2003), and it was then developed to measure the NO_2 and SO_2 emission fluxes from industrial parks (Johansson et al., 2006). In 2008, Mattias Johansson used a mobile mini-DOAS device to quantify the total emission of air pollutants from Beijing and evaluated the measurement error, mainly in terms of the uncertainties in the wind field, experimental setup, sunlight scattering in the lower atmosphere, and DOAS fit error. During the MCMA 2006 field campaign, C. Rivera et al. (2009) used a mobile mini-DOAS instrument to measure the NO_2 and SO_2 emissions of the Tula industrial complex in Mexico and also estimated the flux error. In O. Ibrahim et al. (2010), T. Wagner et al. (2010), and R. Shaiganfar et al. (2011, 2017), air mass factor (AMF), sampling resolution, NOx chemical reactions, and atmospheric lifetime were introduced in order to analyze the emission flux error. The analysis of emission flux error sources has gradually come to focus on the wind field uncertainty, sampling resolution measurement error (GPS error), Slant Column Density (SCD) fit error, AMF error, and other error sources. The aforementioned studies primarily concentrated on regional/industry park emission fluxes, as opposed to point sources.

Different from regional/industry park measuring, point source emission flux can be measured in diverse ways, with different measuring distances, varying sampling resolutions, and so on. Therefore, the error sources and influence factors affecting the flux measurements are different. In order to investigate the impact of these factors and thereby recommend optimum settings for point source flux measuring using mobile DOAS, we performed an in-depth study on the effects of error sources and influence factors on point source emission flux measuring.

There are innate deficiencies in the experimental method used to analyze the emission flux error since there are so many scenarios that need to be verified, and the various factors cannot be well controlled during experiments. Therefore, a convenient way to assist the analysis is sorely needed. In the absence of precise requirements, the simulation method is a good alternative for facilitating the analysis of mobile DOAS emission flux error, given its convenience and feasibility.

Using a model based on Gaussian plume dispersion and the mobile DOAS emission flux measurement method, we here performed a simulation to study the measurement of NOx and SO_2 point source emission flux.

This paper is organized as follows: In Section 2, the methodological framework is presented. In Section 3, the parameters used to drive the simulation are delineated. Section 4 describes the simulation performance and data analysis, Section 5 presents our conclusions, and the Appendix displays the overall simulation results.

2 Methodology and forward model

2.1 Overview of methodology

The NOx and SO_2 emission flux of the point source can be well measured by the mobile DOAS. The equation for calculating the emission flux in the discrete form is expressed as

$$F = \sum_j VCD_j \cdot \vec{u_j} \cdot \vec{n}_j \cdot s_j \quad (1)$$

where F is the emission flux; $VCD_j = SCD_j / AMF_j$, SCD_j is the SCD for mobile DOAS measurements along the measurement route; AMF_j is the Air Mass Factor; $\vec{u}_j$ is the wind field; $\vec{n}_j$ is the vector pointing to the right of the driving direction and parallel to the Earth's surface; and s_j is the sampling resolution. For an isolated point source, the mobile DOAS can measure underneath the plume in downwind direction to quantify the emission flux.

Since individual experiments take place in complex and variable scenarios, in order to investigate the error sources and influence factors that impact the flux measurement error, typical mobile DOAS measurements of the NOx and SO_2 emission fluxes were modeled with the following assumptions:

(1) NOx and SO_2 gas continuously exhaust from an isolated and elevated point source at the position (0 m, 0 m, 235 m). The plume rises approximately 15 m.

(2) The plume is diluted by the wind along the wind direction (x axis). The random movement of air parcels dilute the plume also in the cross-section and in the vertical directions (y axis and z axis).

(3) The topography around the point source is flat and the background concentration of the

pollutants is regarded as zero. In case of non-negligible background concentrations, the VCDs in the plume have to be calculated as difference to the background.

(4) Air turbulence is constant in space and time.

(5) A zenith-sky mobile DOAS measures the gas underneath the plume in the *y*-direction at around noon (see Figure 1). Spectra, GPS data, and wind profiles are available for individual measurements.

(6) The sunlight radiance received by the mobile DOAS instrument is stable.

Figure 1 presents the schematic diagram of the modeled mobile DOAS measurement of a point source.

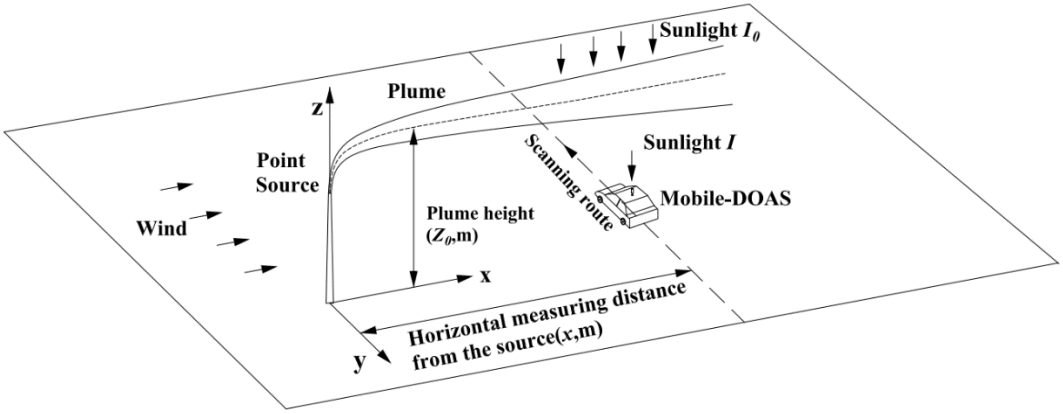

Figure 1. Schematic diagram of the modeled mobile DOAS measurement underneath the plume.

Based on the performance of typical mobile DOAS measurements, a forward model of flux calculations was generated and error analysis performed according to the forward model, as shown in Figure 2.

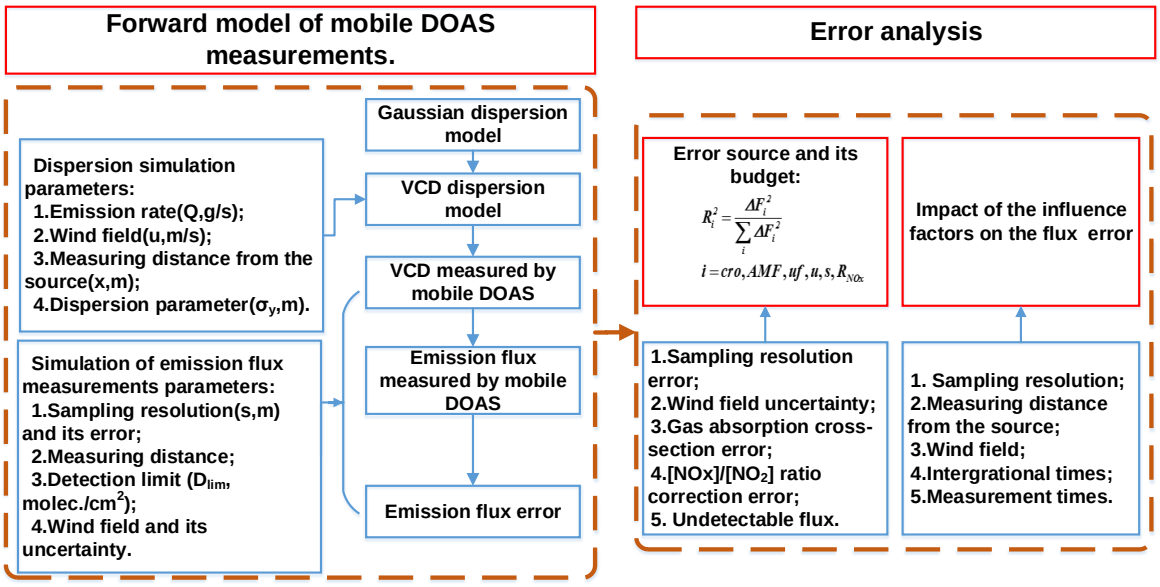

Figure 2. Forward model of mobile DOAS measurements and error analysis.

The forward model of mobile DOAS measurements can be divided into 2 steps:

(1) Dispersion simulation. In this step, a dispersion model is established to generate the vertical column densities (VCDs) measured by the mobile DOAS in the modeled typical measurement.

(2) Simulation of emission flux measurement. After the VCD sequence along the measurement route is generated, the next step is calculating the emission flux and the emission flux error.

Error analysis:

This step concentrates on the error sources and their budget, and the influence factors that affect the emission flux error.

The emission flux and VCD retrieval calculation model can be directly introduced into our forward model, as it has in previous studies. However, some questions concerning the forward model still exist:

(1) Is the existing dispersion model suitable for the mobile DOAS measurement depicted in Figure 1?

(2) How can VCDs be simulated in the same way as mobile DOAS measurements in theory?

(3) Mobile DOAS can measure NO_2 instead of NOx. How can the NO ↔ NO_2 conversion be added to the existing dispersion model in terms of this simulation?

These questions will be explored in Sections 2.2–2.6.

2.2 Description of Gaussian dispersion model

2.2.1 Steady-state Gaussian dispersion model

An appropriate air dispersion model needed to be chosen for generating the forward model of mobile DOAS measurements. Since the concentrations of pollutants at individual points in in the air parcels of the plume under the assumptions we have made can be calculated based on the Gaussian dispersion model (Arystanbekova et al., 2004; Lushi et al., 2010; de Visscher, 2014), we applied the Gaussian dispersion model in this study. The plume, as reflected by the surface due to the ground boundary effect and the dispersion model, can be expressed as Eq.

(2).

$$c(x,y,z)=\frac{DQ}{2\pi u\sigma_y\sigma_z}\exp(-\frac{y^2}{2\sigma_y^2})\cdot\{\exp[-\frac{(z+H)^2}{2\sigma_z^2}]+\exp[-\frac{(z-H)^2}{2\sigma_z^2}]\} \quad (2)$$

where Q is the emission rate (g/s); u is the wind speed (m/s) and the wind direction is along the *x*-direction; σ_y (m) is the dispersion parameter in the *y*-direction; σ_z (m) is the dispersion parameter in the *z*-direction, with σ_y and σ_z dependent on *x*; and H is the plume height (m). $D=\exp(-\varphi\frac{x}{u})$ is the decay term, mainly consisting of the chemical reactions and deposits; φ is the decay coefficient; and $\varphi=\frac{\ln 2}{T_{1/2}}$, in which $T_{1/2}$ is the pollutant half-life in seconds.

The dispersion parameters are determined by the atmospheric stability. The classification of atmospheric stability, which was created by Pasquill and Gifford and is widely used, sorts atmospheric stability into 6 classes ranging from A–F (de Visscher, 2014). We only considered the classifications under strong solar radiation (see Table 1) in this study.

Table 1. Pasquill–Gifford atmospheric stability classifications.

Wind Speed at 10m above the surface (m/s)	Strong Solar Radiation class
< 2	A
2~3	between A and B
3~5	B
5~6	C
>6	C

A: very unstable; B: moderately unstable; C: slightly unstable

Based on the atmospheric stability class and the terrain type surrounding the emission point, the parameters σ_y and σ_z can be calculated. Since we assumed the surrounding area to be flat, rural terrain, the σ_y and σ_z parameters could be calculated using Briggs's (1973) formulas, listed in Table 2.

Table 2. Rural area air dispersion parameters (Briggs, 1973).

Stable classes	$\sigma_y(x)$	$\sigma_z(x)$
A	$0.22x(1+0.0001x)^{-0.5}$	$0.2x$

B	$0.16x(1+0.0001x)^{-0.5}$	$0.12x$
C	$0.11x(1+0.0001x)^{-0.5}$	$0.08x(1+0.0002x)^{-0.5}$

in which x is the horizontal distance from the source, m.

It should be noted that Briggs's equations are only suitable under the condition of x lower than 10 km. The dispersion in the wind direction is negligible in comparison with the advection when the wind speed is high, or for weak turbulence (de Visscher, 2014). In addition, the model accuracy significantly decreases in the case of wind speeds < 1 m/s. The critical wind speed for the Gaussian dispersion model is about 1.2m/s (de Visscher, 2014). For high wind speed, the effect of undetectable flux becomes very important (see e.g. results in Fig. 8). Thus for the general cases considered here measurements under high wind speed are not recommended. Only for very high emissions and close to the source (< 1km), measurements for high wind speeds might be meaningful, but such situations might be rare. Since our study focuses on the general cases, we limit it to wind speeds < 8m/s, because in the range up to 8m/s the general dependencies become obvious. Therefore, the wind speed range in our simulation is between 1.2 m/s and 8 m/s. The distance in our simulation is within 10km.

2.2.2 NOx dispersion

Eq. (2) is suitable for SO_2 dispersion, while for NOx, mobile DOAS can only measure NO_2 effectively. Hence, Eq. (2) should be adjusted for NO_2 dispersion based on NOx atmospheric chemical reactions. In this study, we did not take Volatile Organic Compounds (VOCs) into consideration; thus, a NOx balance would not be broken. Moreover, we assume that no NOx is presented in the ambient air and no O_3 is consumed in the reaction with NO. In most cases, both assumptions are reasonable, especially as long as the background NOx concentration has no strong spatial-temporal variation. However, for very high emission rates, the assumption that no O_3 is consumed in the reaction with NO might be violated (a simple criterion to identify such cases might be to check whether the NOx mixing ratios are higher than the ambient O_3 mixing ratios). If this is the case, the conversion of NO to NO_2 will be delayed. The typical reactions of NO, NO_2, O_3, and O_2 in the air parcels of the plume are:

$$NO_2 + h\nu \rightarrow NO + O(^3P) \quad \text{(reaction 1)}$$

$$O_2 + O(^3P) \rightarrow O_3 \quad \text{(reaction 2)}$$

$$NO + O_3 \rightarrow NO_2 + O_2 \quad \text{(reaction 3)}$$

The reaction rates of reactions 1, 2 and 3 form a cyclic reaction. The reaction rate of NO_2 is:

$$r_{NO2} = -j_3[NO_2] + k_5[NO][O_3]_t \quad (3)$$

where [gas] stands for the concentration of a particular gas; $[O_3]_t$ is the O_3 concentration in the air parcels of the plume at time *t*; *t* is the time period after NOx is emitted into the atmosphere. We assumed that at the beginning there is no O_3 in the air parcels of the plume. During the mixing with outside air, the O_3 concentration within the air parcels increases. For simplicity, we assumed that the O_3 concentration is the same everywhere in a transect of the plume. j_3 is the NO_2 photochemical rate constant, equal to approximately 8×10^{-3} s^{-1}; and k_5 is the rate constant of reaction 3, equal to approximately 1.8×10^{-14} $cm^3 molecules^{-1} s^{-1}$ (de Visscher, 2014). It should be noted that these rates are for a temperature of 25 ℃. Fortunately, they are not sensitive to temperature, so temperature sensitivity did not need to be considered.

The [NOx]/[NO_2] ratio depends on the mixing ratio of O_3 inside the plume. The mixing ratio of O_3 within the air parcel of the plume can then be estimated as:

$$[O_3]_t = [O_3]\frac{V_t - V_0}{V_t} = [O_3]\frac{S_t\Delta t - S_0\Delta t}{S_t\Delta t} = [O_3](1 - \frac{S_0}{S_t}) \quad (4)$$

where V_0 is the initial gas volume of the plume and S_0 is the initial gas cross-section of the plume; while V_t is the gas volume of the plume at time *t* and S_t is the gas cross-section of the plume in the atmosphere at time *t*. Here, $[O_3]$ is the ambient O_3 concentration. The NO_2 concentration inside the plume at time *t* is given by:

$$[NO_2]_t = \int_0^t r_{NO2} dt \quad (5)$$

Since the NO_2 initial concentration was very low, we assumed the NO_2 initial concentration

223 $[NO_2]_0 = 0$. Consequently, $[NOx]_t = [NO]_0$ (with no decay).

224 The [NOx]/[NO_2] ratio at time *t* is:

225 $$R_{NOx} = \frac{[NOx]_t}{[NO_2]_t} \tag{6}$$

226 Different from SO_2, the number of NOx molecules is conserved, as opposed to their mass.
227 The NOx dispersion model should thus be expressed as:

228 $$c_{NOx}(x,y,z) = \frac{DQ_{mNOx}}{2\pi u\sigma_y\sigma_z}\exp(-\frac{y^2}{2\sigma_y^2})\cdot\{\exp[-\frac{(z+H)^2}{2\sigma_z^2}]+\exp[-\frac{(z-H)^2}{2\sigma_z^2}]\} \tag{7}$$

229 where $Q_{mNOx} = \frac{Q\cdot NA}{m_{NOx}}$. m_{NOx} is the mean molar mass of the initial NOx and NA is Avoga-
230 dro's constant of 6.02×10^{23} molecules mol^{-1}. Substituting Eq. (6) into Eq. (7), the NO_2 dis-
231 persion model can then be expressed as:

232 $$c_{NO2}(x,y,z) = \frac{c_{NOx}(x,y,z)}{R_{NOx}} \tag{8}$$

233 **2.3 VCD dispersion model**

234 As discussed above, mobile DOAS retrieves the VCD, while results of the dispersion mod-
235 el are point concentrations of the air parcels. Based on the definition of VCD, we integrate the
236 concentration along the vertical direction, i.e., the *z*-direction from the ground to the upper
237 troposphere, as in:

238 $$\begin{aligned} VCD(x,y) &= \int_0^{+\infty} Dc(x,y,z)dz = \frac{DQ}{\sqrt{2\pi}u\sigma_y\sigma_z}\int_0^{+\infty}\{\exp[-\frac{(z+H)^2}{2\sigma_z^2}]+\exp[-\frac{(z-H)^2}{2\sigma_z^2}]\}dz \\ &= \frac{DQ}{\sqrt{2\pi}u\sigma_y}\exp(-\frac{y^2}{2\sigma_y^2}) \end{aligned} \tag{9}$$

239 Eq. (9) is suitable for SO_2. For NOx, the VCD dispersion is

240 $$VCD_{NOx}(x,y) = \frac{DQ_{mNOx}}{\sqrt{2\pi}u\sigma_y}\exp(-\frac{y^2}{2\sigma_y^2}) \tag{10}$$

241 The NO_2 VCD dispersion model is

242 $$VCD_{NO2}(x,y) = \frac{VCD_{NOx}(x,y)}{R_{NOx}} \tag{11}$$

243 Since NOx disperses along the wind direction and R_{NOx} is a function of *t*, this means that
244 R_{NOx} also varies with distance. The detailed relationship between the distance and R_{NOx} will

be discussed in subsection 4.4. Eqs. (9), (10), and (11) lay the mathematical foundation of the VCD distribution model for mobile DOAS measuring.

2.4 VCD measured by mobile DOAS

As shown in Figure 3, the flux of the plume cross-section can be calculated using the following equation:

$$\Delta F_j = u \cdot \int_l VCD(x, y) ds \tag{12}$$

ΔF_j is the flux along the measurement route l in theory. For mobile DOAS measurement, ΔF_j should be given by Eq. (13)

$$\Delta F_j = VCD_j \cdot u \cdot s_j \tag{13}$$

where s_j is the distance between 2 measuring points and VCD_j can be derived from the spectrum of measurement j. Based on Eqs. (12) and (13), VCD_j can be expressed by Eq. (14)

$$VCD_j = \frac{1}{s} \int_l VCD(x, y) ds \tag{14}$$

Eq. (14) indicates that the VCD_j derived from individual mobile DOAS measurements is the average of $VCD(x,y)$ along the measurement route. The discretization of the VCD can significantly affect the emission flux error and will be discussed in Section 4.1.

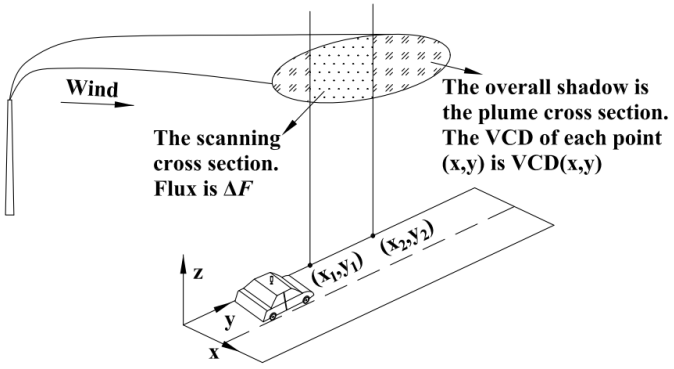

Figure 3. Model of VCD measured by mobile DOAS

2.5 Description of emission flux measured by mobile DOAS

Since the SO_2 lifetime scale is longer than the dispersion time scale, a decay correction is not needed for SO_2, but for NOx it can be necessary. The SO_2 emission flux is then using Eq. 1 to calculate, while the NOx emission flux is:

$$F_{NOx} = \frac{R_{NOx}}{D} F_{NO2} \quad (15)$$

In fact, the decay correction for NOx should be applied for cases with low wind speeds, while the effect for high wind speeds is very small.

2.6 Measurement errors of emission flux

Emission flux measurements errors not only arise from measurement errors but also depend on other factors, such as wind speed, measuring distance, [NOx]/[NO_2] ratio and the sampling resolution.

Since the VCD is inversely proportional to the wind speed (Eqs.9 and 10), the higher the wind speed is, the lower the VCD. This means more measurements at the edge of plume would be under the detection limit at higher wind speeds causing more undetectable flux. The VCD is also inversely proportional to measuring distance (Eqs.9 and 10). This means that the undetectable flux increase with measuring distance. Since the [NOx]/[NO_2] ratio depends on the measuring distance (see figure 10), a large [NOx]/[NO_2] ratio correction error occurs when the measuring distance is small. Finally, the sampling error can be reduced with improved sampling resolution.

The emission flux measurement errors by mobile DOAS have several sources: SCD fit errors, AMF errors, wind field uncertainties, and sampling resolution measurement errors (Johansson et al., 2008, 2009; Wagner et al., 2010; Ibrahim et al., 2010; Shaiganfar et al., 2011, 2017; Rivera, et al., 2012).

The uncertainty of the derived SCD from the DOAS fit has a random and systematic part. For the random part it can be assumed that in general it cancels out (in combination with the sampling resolution error it can have a very small contribution). Thus, its direct effect on the total flux error is neglected in the following. However, from the fit error also the detection limit is estimated. For SCDs below the mobile DOAS detection limit, undetectable SCDs result in undetectable flux and therefore the fit error indirectly contributes to the total flux error.

The systematic part of the SCD error caused by the uncertainty of the trace gas absorption cross-section is independent from the SCD fit error and is therefore included as an additional term in the total flux error calculation.

We assume that these errors are random, have a Gaussian distribution and are independent of each other. Then the total relative error of the emission flux is given by:

$$E_{total} = \frac{F_{err}}{D \cdot Q} \times 100\% = \frac{\sqrt{\Delta F_{cro}^2 + \Delta F_{uf}^2 + \Delta F_{AMF}^2 + \Delta F_u^2 + \Delta F_s^2}}{D \cdot Q} \times 100\% \quad (16)$$

where F_{err} is the total flux error; ΔF_{cro} is the flux error introduced by gas absorption cross-section error; ΔF_{uf} is the undetectable flux; ΔF_{AMF} is the flux error introduced by AMF errors; ΔF_u is the flux error introduced by wind speed uncertainty. The wind direction uncertainties play a smaller role in point source flux measuring error (and can be derived from geometry), thus the uncertainties caused by the wind field are dominated by the wind speed uncertainties. The error term of the wind direction uncertainty is therefore removed. ΔF_s is the emission flux error introduced by sampling resolution measurement error and it can be neglected (see section 4.1).

Eq. (16) is appropriate for SO_2. With regard to NOx, the NOx flux error is also introduced by the decay correction and the [NOx]/[NO_2] ratio correction error. Hence, the NOx flux relative error is:

$$E_{NOx} = \frac{F_{err}}{D \cdot Q} \times 100\% = \frac{\sqrt{\Delta F_{R_{NOx}}^2 + \Delta F_{cro}^2 + \Delta F_{uf}^2 + \Delta F_{AMF}^2 + \Delta F_u^2 + \Delta F_s^2}}{D \cdot Q} \times 100\% \quad (17)$$

where ΔF_D is the flux error due to decay correction, and ΔF_{RNOx} is the flux error due to [NOx]/[NO_2] ratio correction.

In order to quantify the contributions/budget of individual error sources, the ratios are calculated as Eq. (18)

$$R_i^2 = \frac{\Delta F_i^2}{F_{err}^2} \quad (18)$$

where *i* represents the individual error sources. Note that $\sum_i R_i^2 = 1$.

3 Parameter assumption and numerical simulation

In Section 2, the forward model for mobile DOAS measurements of emission flux was es-

tablished. In this section, reasonable values of the parameters in the forward model are discussed and prepared in order to drive the forward model.

For most factories, including power plants, the emission rates of NOx and SO_2 are different. Since a higher emission rate is an ideal condition for mobile DOAS measurements, higher emissions could be outside the scope of our study. Therefore, the emission rate that we simulated was < 200 g/s, and we set the Q value within this range. Since the Gaussian dispersion model is appropriate for moderate wind speed and scale, the wind speed was set to range from 1.2~8 m/s and the dispersion distance was approximately 0~10 km. Given the car speed and mobile DOAS spectrometer integration times t_{int}, the sampling resolution was set from 5–500 m. The NOx mean daytime lifetime is approximately 5 h ± 1 h (Spicer, 1982), while the SO_2 daytime lifetime is more than 1 day (S. Beirle, 2014). Compared with the dispersion time scale, the SO_2 daytime lifetime uncertainty could be neglected. When time approaches infinity, the NOx reaction steady-state could be determined by ambient [O_3] according to Eq. (5). We here assumed a typical [O_3] value 1.389×10^{12} molecules cm^{-3} thus the steady-state [NOx]/[NO_2] ratio is 1.32. The [NOx]/[NO_2] ratio inside the air parcel of the plume varying with the distance could be determined by Eqs. (5), (6), (7) and (8).

The SCD error can mainly be attributed to the DOAS fitting error of the SCD and the trace gas absorption cross-section error. Previous studies have indicated that the typical fit errors of NO_2 and SO_2 SCDs are $\pm(1\sim4)\times10^{15}$ molecules cm^{-2} and $\pm(1\sim6)\times10^{15}$ molecules cm^{-2}, respectively (Wagner et al., 2011; Wang et al., 2014; Wu et al., 2018; Davis et al., 2019). Thus in this study, we set the fit error of NO_2 and SO_2 to be $\pm2.5\times10^{15}$ molecules cm^{-2} and $\pm4\times10^{15}$ molecules cm^{-2} (1σ error), respectively. Here in addition, we use the 2σ values as detection limit (see e.g. Alicke et al., 2002; Platt and Stutz, 2008). The absorption cross-section errors are less than 3% for NO_2 and less than 2.4% for SO_2 (Vandaele et al., 1994, 1998). In this study, we set the total SCD error from gas absorption cross-section errors to 5% (Theys, et al., 2007) for both NO_2 and SO_2. Of course, these values are only rough estimates, but they are useful to investigate the general dependencies of the total flux error.

VCDs are derived from SCDs applying AMF. We calculated AMFs using the Monte Carlo

atmospheric radiative transfer model McArtim (Deutschmann et al., 2011). For that purpose, we calculated 3-D box-AMF for different aerosol loads and solar zenith angle (SZA). It should be noted that the application of 3-D box-AMF (in contrast to 1-D box-AMF) is important for the measurements considered in our study, because horizontal extension of the plumes perpendicular to the wind direction is rather short (compared to the average horizontal photon path lengths). Our simulations indicate that, for a plume height around 250m, the AMF is typically between 1.05 and 1.3. The higher values are for high aerosol load and high SZA (here only measurements below 75 °are considered), the lower values are for low aerosol load and low SZA. In this study, we use an AMF of 1.15 and assume an AMF error of ±10%. For layer heights below 50m, the AMF is around 1.03 and the AMF error can be neglected.

The sampling resolution measurement error is primarily attributed to the drift of GPS. However, flux error due to GPS drift could be neglected (see subsection 4.1).

The flux error due to wind field uncertainty mainly comes from wind speed uncertainty. In order to quantify the wind speed uncertainties, the 1-month wind profile data at the height of 250 m during the time period 9:00~16:00 from 1 April–30 April 2019 were derived from the Doppler wind profile radar located in Shijiazhuang (38.17 ℃N, 114.36 ℃E). The average wind fields and standard deviations were calculated for each hour, as shown in Figure 4. Two-order polynomials were applied in order to derive the function of standard deviation versus average value for both wind speed and wind direction. Some sample values calculated using these polynomials are listed in Table 3. Table 4 lists all the simulation parameters of NOx and SO_2 that were required.

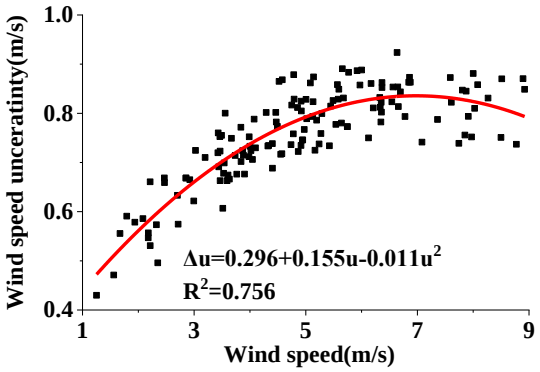

Figure 4. Polynomial fitting of the uncertainty between wind speed and wind direction.

Table 3. Wind speed uncertainty and wind direction uncertainty after polynomial fitting.

wind speed(m/s)	wind speed uncertainty(±,m/s)
1.2	0.466
2	0.562
3	0.662
4	0.740
5	0.796
6	0.83
7	0.842
8	0.832

Table 4. Simulation parameters and data range of NOx and SO_2.

Parameter	Values
Emission rate(g/s)	10, 30, 50, 100 , 150, 200
Wind speed(m/s)	1.2, 2,3, 4, 5, 6, 7, 8
Measuring distance(km)	0~10km
Sampling resolution	5~500m, initial integration times t_{int}
Fit error(molecules cm^{-2}) Detection limit(molecules cm^{-2})	NO_2: ~2.5×10^{15}; SO_2: ~4×10^{15} NO_2: 5×10^{15}; SO_2: 8×10^{15}
AMF and its error	1.15±10%
Gas absorption cross-section errors	±5%
Average atmosphere lifetime	NOx:5h±1h; SO_2: more than 1 day
R_{NOx}	R_{NOx} inside the plume is calculated by Eqs. (5), (6), (7) and (8). R_{NOx} in NOx reaction steady-state is 1.32.

The parameters listed in Table 4 were applied in the forward model in order to perform the simulation. The simulation results are shown in Figures 25 and 26 of the Appendix.

4 Analysis of emission flux errors measured by mobile DOAS based on the forward model

Figures 25 and 26 in the Appendix show that the modeled relative errors of NOx and SO_2 emission flux varied with sampling resolution and distance from the point source under different wind speeds and emission rates. Some overall features can be derived from these figures. Therefore, typical cases were selected in order to discuss the overall features based on

several key factors.

4.1 Sampling resolution and its error

Sampling resolution variation impacts on the error combination and propagation and its error is an error source.

Sampling resolution is derived from GPS records in actual measurement. The typical uncertainty of the GPS readings is <1.5m. For measurements with small sampling resolutions the GPS error can thus cause relatively large uncertainties for the flux contributions from individual measurements (Eq. 1). However, even for small sampling resolutions the GPS errors of neighboring flux contributions almost completely cancel each other. Thus, the contribution of the GPS error to the flux calculation (Eqs. 16 and 17) can be neglected.

In actual measurements, if one distance is too long, and this happens to be inside the plume, while the next distance is too short but is already outside the plume, the flux will be overestimated in spite of the fact that the sum of the two distances has only a small error. In this case, the sampling error becomes important. The sampling error is largest when the sampling resolution is large. Thus a small and uniform sampling resolution is particularly important.

In order to discuss the dependence of flux error on sampling resolution, some data were extracted from the Appendix and plotted in Figure 5. This figure shows the increase of relative error with increasing sampling resolution. It should be noted that the smaller the sampling resolution, the more data the mobile DOAS will sample. This directly leads to the inclusion of more data in the emission flux calculations, resulting in the lower emission flux error. However, when far from the source, the plume with narrows quickly (see section 4.2). Appling different sampling resolution is no longer feasible. Therefore, the sampling resolution can only work effectively when the measurements are not far from the source.

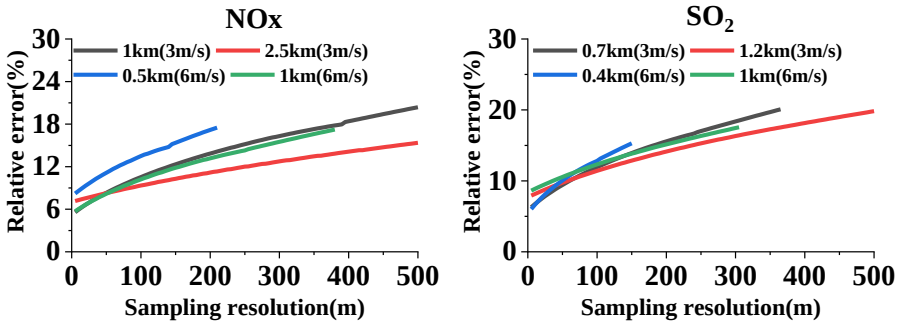

Figure 5. Dependence of relative errors on sampling resolution (Q = 100 g/s, u = 3 m/s and 6 m/s, at different measuring distances).

The impact of sampling resolution on emission flux error is noticeable. In terms measurement efficiency, the sampling resolution should not be too small. Also to avoid large errors and sampling errors, large resolution is not recommended. Therefore, we recommend the proper sampling resolution to be between 5 m and 50 m. Larger resolutions may also be viable, but > 100 m is not recommended.

4.2 Measuring distance from the source

Measuring distance is not an error source, but affects the dispersion and NOx chemical reactions, further adding to the emission flux error. Figure 6 presents typical examples of relative errors varying with distance at a resolution of 20 m. Wind speeds of 3 m/s and 6 m/s were utilized in this example. The overall feature shown in all of the sub-figures of Figure 6 is the rapid decrease and then quick increase of the relative error with measuring distance. Different factors lead to the large errors at small and large distances.

First, we analyzed NOx and SO_2 emission flux errors for a large measuring distance. The large distance results in the dramatic decrease of SCDs due to dispersion and decay along the plume transport path. The SCDs can be lower than the detection limit of mobile DOAS measurements, resulting in a portion of the undetectable flux. Because of dispersion, the plume widths with SCDs above the detection limit and thus the detectable fluxes decrease significantly with distance, even dropping to zero, as shown in Figure 6. This causes the relative error to increase at large measuring distances.

Second, we analyzed NOx and SO_2 emission flux errors in the case of a small measuring distance. Figure 6 indicates that the error is large and decreases rapidly with increasing measuring distance when close to the source. As discussed in Section 4.1, if more measurement data are included in the calculations of flux, the relative error can decrease. When the measuring distance is small, the number of samples can dramatically decrease. For SO_2, the relative error can increase significantly when the measurements are close to the point source. For NOx, the relative error is also affected by chemical reactions, this phenomenon that we will

discuss in Section 4.4.

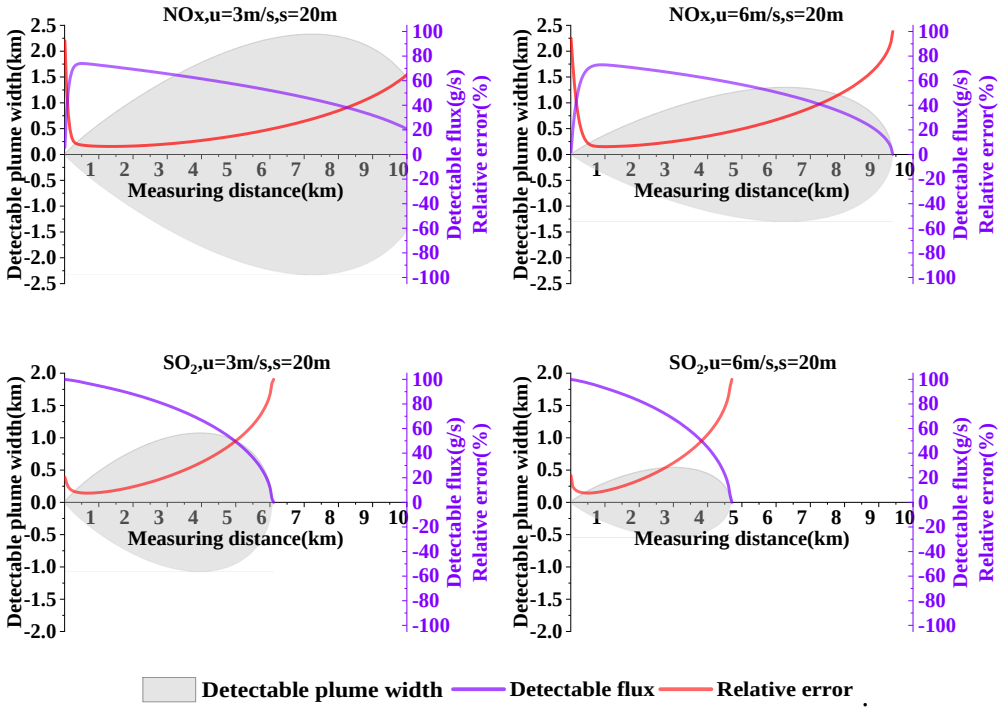

Figure 6. Variation of NOx and SO_2 flux relative errors with distance, using Eqs. (16) and (17) (Q = 100 g/s, setting the sampling resolution *s* = 20 m and the wind speed to 3 m/s and 6 m/s).

4.3 Wind fields and their uncertainties

Wind fields can impact both the gas dispersion (Eqs. 2, 9 and 10) and the calculation of emission flux (Eqs. 1 and 15). In terms of dispersion, wind speed affects gas VCD (Eqs. 9 and 10). In terms of flux calculation, the temporal and spatial uncertainty of wind fields can contribute to emission flux calculation errors. Therefore, the effects of wind fields are discussed based on these 2 factors in this section.

Figure 7 displays the variations of the relative errors of NOx and SO_2 with wind speed at different distances. The emission rate Q and the sampling resolution are chosen as 100 g/s and 20 m, respectively. Figure 7 indicates the different features of relative error for wind speeds at small and large measurement distances. The relative error of NOx increases with increasing wind speed at different distances, while the SO_2 relative error for measurements at small distances exhibits a trend opposite that of the large distance measurements. The causes of the different relationships at small and large measurement distances are discussed in subsection 4.3.1.

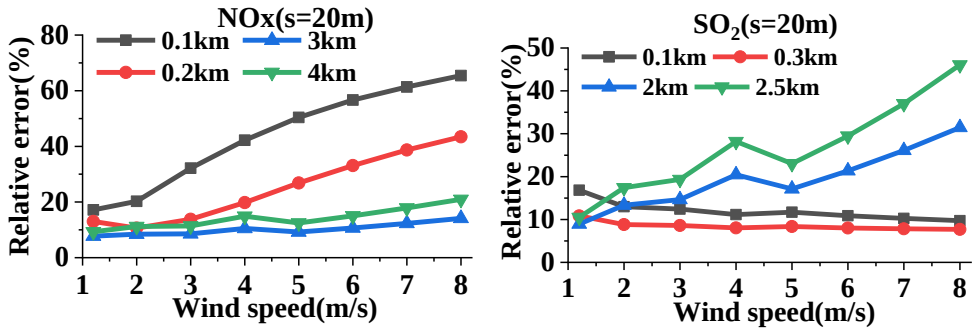

Figure 7. Relative errors of NOx and SO_2 emission flux changes with wind speed at different measurement distances (Q = 100 g/s, sampling resolution *s* = 20 m).

4.3.1 Effects of different wind speeds on measurements at small and large measurement distances

Since the NOx and SO_2 flux measurement errors of different wind speeds are very different at small and large measurement distances, we discuss them separately.

4.3.1.1 SO_2

We first analyzed the effect of different wind speeds on the SO_2 emission flux error.

Since VCDs decrease with increasing wind speed (Eqs. 9, 10 and 11), more SCDs would be below the detection limit of mobile DOAS at high wind speeds. Hence, the contribution of undetectable SCDs to the error of flux calculations depends on wind speed. In addition, since wind fields are input into the calculations of emission flux (Eqs. 1 and 15), their uncertainties can contribute to the flux measurement error. In order to investigate the contributions of undetectable ambient VCDs and the influence of wind field uncertainties in flux measurement, the ratios R_{uf}^2 (R^2 of the undetectable flux) and R_u^2 (R^2 of the wind speed uncertainty) calculated using Eq. (18) are shown in Figures 8c and 8d for different wind speeds and measurement distances.

Again, we first analyzed the measurements at large distances. The undetectable VCDs dominate the effect of wind fields on the error of flux calculations when the measurement distance is large. As shown in Figures 8d, undetectable flux dominates the flux errors when measuring at large distance. The R_{uf}^2 becomes greater with larger wind speeds, for large measurement distances. For large measurement distances, as shown in Figures 8c and 8d.

Therefore, undetectable VCDs dominate the effect of wind fields on the error of flux calculations when the measurement distance is large. Since VCDs decrease with increasing wind speeds, the flux error associated with undetectable VCDs should be increased with wind speed. This relationship explains the phenomenon that the relative error of emission flux increases with increasing wind speed for large measurement distances.

Next, the measurements at small distances were analyzed. Figures 8c and 8d indicate that R_{uf}^2 is much lower than R_u^2 for short measurement distances. The wind field uncertainty dominates the effect of wind fields on the flux calculation errors. Meanwhile, since the relative uncertainty of the wind field decreases with increasing wind speed, the emission flux error decreases with increasing wind speed for short measurement distances, as shown in Figure 6.

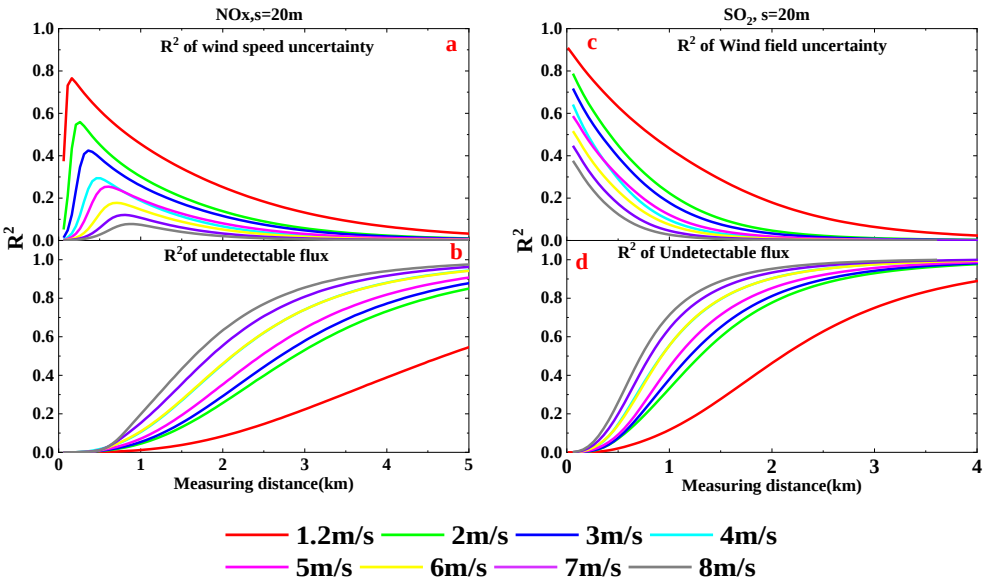

Figure 8. Wind speed uncertainty ratio squared R_u^2 (**a** and **c**) and undetectable emission flux ratio squared R_{uf}^2 (**b** and **d**) of NO_2 and SO_2 emission flux measurement error changes with measurement distance for different wind speeds (Q = 100 g/s, sampling resolution *s* = 20m).

4.3.1.2 NOx

We next analyzed the effect of different wind speeds on NOx emission flux error, as shown in Figures 9a and 9b.

The effects of different wind speed dispersions on NOx emission flux error are similar to SO_2, i.e., Figures 8b and 8d, indicating that the effects of wind speed dispersion are analogous.

The effect of wind field uncertainty is much different from SO_2, however, especially when the measurements are very close to the source. When very close, wind field uncertainty influence increases and then decreases with distance. Compared with SO_2, the decreasing trend of NOx in the case of far measurement distances is also similar, but the increasing trend is very different. This implies that NOx measurements close to the source have another main potential error source, which we will investigate in Section 4.4.

The 4 subfigures in Figure 8 share the common characteristic that the R^2 lines have intersections between 4 m/s and 5 m/s. This implies that the wind field uncertainty effect and the wind field dispersion effect are distinguished between 4 m/s and 5 m/s. In actual measurements, undetectable VCDs cannot be well quantified. Therefore, we recommend the proper wind speed for mobile DOAS to be < 4 m/s. The appropriate lower wind speed in this study was 1.2 m/s, But the Gaussian plume model we used becomes increasingly inaccurate when wind speeds are under 1m/s. Thus, we recommend a proper wind speed of 1–4 m/s.

4.3.2 Error budget of undetectable flux, uncertainties of wind speed

The remaining question is what flux error budget is associated with the wind speed. From Section 2.6 we know that Wind field uncertainties mainly come from the wind speed uncertainties. Undetectable flux is the result of SCDs below the detection limit, but the main drivers of R_{uf}^2 increasing trend along the wind direction is the wind dispersion. Figure 9 presents the changes of R_u^2 and R_{uf}^2 of NOx and SO_2 with distance for different wind speeds, 3 m/s and 6 m/s.

As for SO_2, the wind field influence contributes most of the emission flux error from wind field uncertainty, in conjunction with wind dispersion. Furthermore, contributions from wind speed uncertainty in the emission flux error are also presented in Figure 9. This demonstrates that wind speed uncertainty dominate the flux error when close measuring.

With regard to NOx, the wind speed influence is similar to SO_2 when measuring far from the source and very different when measuring close to the source. As discussed above, mobile DOAS can only measure the NO_2, as opposed to the NOx. The amount of NO_2 yield determines the mobile DOAS measurement result, and thus that of the NOx flux measurement error, especially when measuring very close to the source.

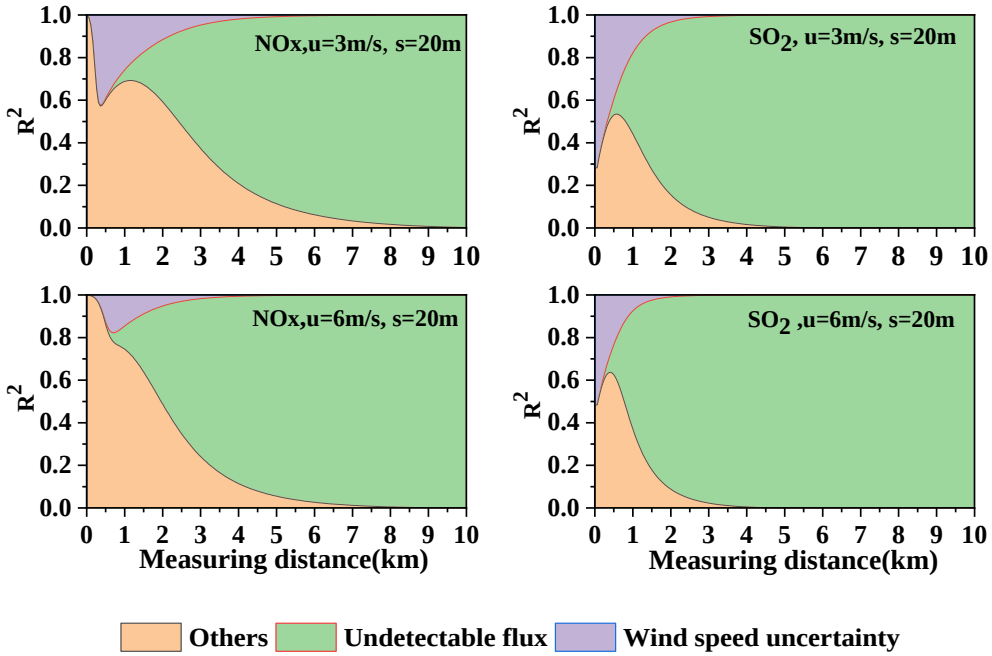

Figure 9. Changes of R_u^2 and R_{uf}^2 of NOx and SO_2 emission flux measurement errors with measurement distance for different wind speeds (Q = 100 g/s).

4.4 NOx chemical reactions

In Section 4.2, we left unanswered the question as to why the NOx flux error is very large when very close to the source (see Figure 6). In this section, we will investigate the reason for this phenomenon.

Stacks mainly exhaust NO, which then transforms into NO_2 in a few minutes due to chemical reactions. Since NOx disperses along the wind direction, this means that the [NOx]/[NO_2] ratio varies with distance. With O_3 mixing to the air parcels of the plume continually, more NO_2 would yield and [NOx]/[NO_2] ratio decreases with the distance before the NOx reaction steady-state. For readability, we here show the increasing trend of [NO_2]/[NOx] ratio along the distance in Figure 10a.

In actual measurements, especially for elevated point sources, the dependence of the [NOx]/[NO_2] ratio on the distance from the air parcels of the plume is difficult to measure. The [NOx]/[NO_2] ratio could e.g. be measured by an in situ instrument on the ground. However, in some cases the plume might not reach the ground. And even if it reaches the ground the measured [NOx]/[NO_2] ratio is probably not representative for the whole plume. Furthermore, also the ambient [O_3] could be measured, which would help to constrain the

[NOx]/[NO_2] ratio. But also if O_3 measurements are available, the calculation of the [NOx]/[NO_2] ratio will have its uncertainties, and the derived [NOx]/[NO_2] ratio will again not be representative for the whole plume. Thus in our study, we calculate the [NOx]/[NO_2] ratio based on the dispersion model with some additional assumptions which are outlined in the text. In this way we can derive the general dependencies of the [NOx]/[NO_2] ratio on the plume distance and apply a corresponding correction. However, for the NOx flux calculations, even after the application of the [NOx]/[NO_2] ratio correction factor, substantial flux errors near the source might occur.

Subfigure b in Figure 10 displays the R^2_{RNOx} value of the [NOx]/[NO_2] ratio correction error. The larger the [NOx]/[NO_2] ratio, the larger the R^2_{RNOx} value of the [NOx]/[NO_2] ratio correction. This causes the R^2_{RNOx} to increase, to as high as 1, when near the source. Also, from the R^2_{RNOx} value we discovered that the [NOx]/[NO_2] ratio correction error is the main error source when close to the emission source. Hence, the main flux error source near the emission source is the [NOx]/[NO_2] ratio correction error.

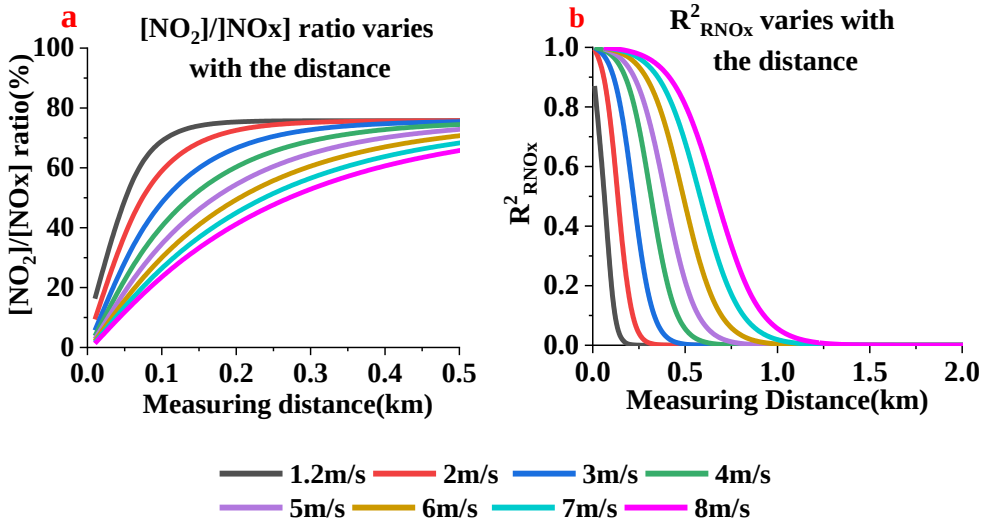

Figure 10. variation of [NO_2]/[NOx] ratio (**a**) R^2_{RNOx} with distance (**b**) at different wind speeds (Q = 100 g/s).

Since we know that the [NOx]/[NO_2] ratio correction error is the main error source near the emission source, developing ways to avoid or minimize this error is our goal.

In real-world experiments, accurately measuring NOx flux requires NOx to reach a steady-state. According to Eq. (3), when time approaches infinity, the NO_2 reaction rate r_{NO2} approaches 0, indicating that NOx reaches a steady-state. In theory, steady-state NOx is an ideal condition for measuring NOx flux. Infinite time, however, is not our expectation. If we regard $r_{NO2} = 0.05 r_{\max}$ as the approached steady-state, the approached steady-state time could be attained, as well as the approached steady-state distance. $r_{\max}$ is defined as the theoretical NO_2 maximal reaction rate, which is $r_{NO2} = k_5[NO]_0[O_3]$. Figure 11a displays the variation of $\frac{r_{NO2}}{r_{\max}}$ with time and Figure 11b displays the approached steady-state distance.

In order to investigate the feasibility of our recommendation, we used the following equation for analysis:

$$E_{RNOx} = \frac{\Delta F_{RNOx}}{DQ} \times 100\% \tag{19}$$

where ΔF_{RNOx} is the flux error resulting from the [NOx]/[NO_2] ratio correction at the approached steady-state distance. E_{RNOx} is used rather than R^2 because R^2 only represents the error source contribution/budget. For example, the R^2 value of the [NOx]/[NO_2] ratio correction error is 0.9, while the total relative error is only 10%. In this case, it seems that we cannot accept the high R^2, although the total relative error is acceptable. Therefore, in our judgment, using E_{RNOx} is an advantage.

The E_{RNOx} values at the approached steady-state distance for different wind speeds and emission rates were calculated, and the results are presented in Figure 11c. From this figure, we can infer that E_{RNOx} is approximately 5%, which is very low. This indicates that the flux error resulting from the [NOx]/[NO_2] ratio correction at the approached steady-state distance is very small and can thus be regarded as negligible.

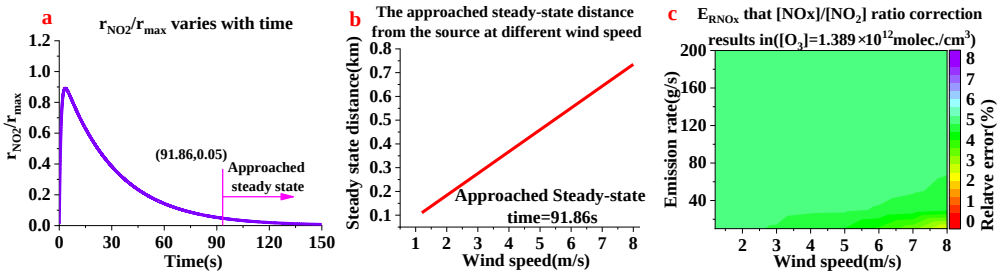

Figure 11. variation of r_{NO2}/r_{max} with time (**a**), NOx steady-state distance from the source (**b**) and E_{RNOx} values (**c**) under different emission rates and wind speeds ([O_3]= 1.389 × 10^{12} molecules cm^{-3}).

According to Eq. (3), r_{NO2} depends on [O_3]. Hence, we also calculated the NOx steady-state distance and E_{RNOx} under different [O_3]. The E_{RNOx} was also approximately 5% under different [O_3], as shown in Figure 12. The dependence calculation demonstrates that E_{RNOx} is also very small under different [O_3]. Consequently, regarding $r_{NO2}=0.05r_{max}$ as the approached steady-state seems to be acceptable.

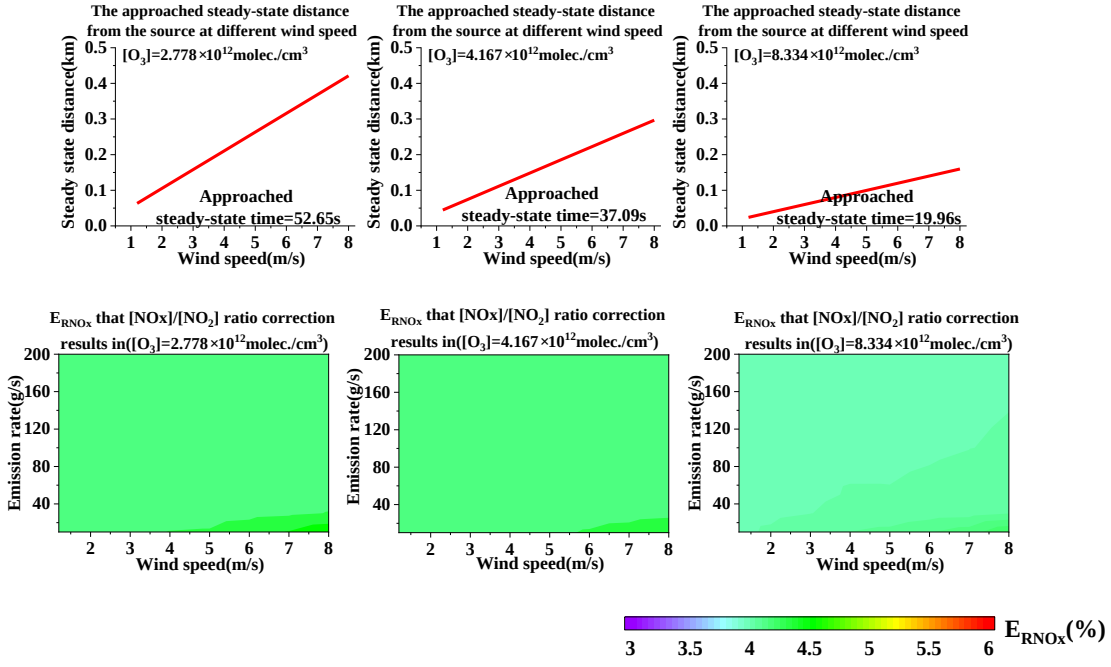

Figure 12. NOx approached steady-state distance from the source (upper plot) and E_{RNOx} values (bottom plot) under different emission rates, different wind speeds, and different [O_3].

In summary, when very close to the emission source, the main flux error source is the [NOx]/[NO_2] ratio correction error. In order to avoid or minimize this error, we recommend $r_{NO2}=0.05r_{max}$ as the approached steady-state, in which case the approached steady-state

603 distance is the starting measurement distance. The overall distances for different [O_3] concen-
604 trations were also simulated as a reference for the DOAS measurement of NOx point source
605 emissions, as shown in Figure 13.

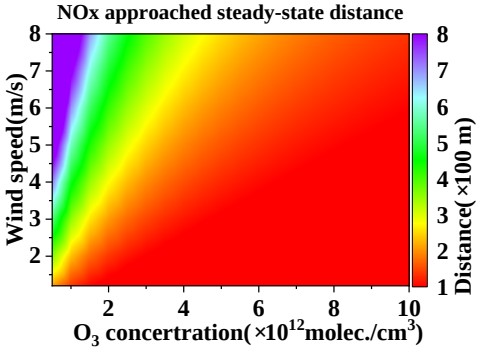

606
607 Figure 13. NOx steady-state distance from the source for different [O_3] concentrations ($r_{NO2} = 0.05 r_{\max}$).
608

609 **4.5 Undetectable flux**

610 As discussed in sections 4.3, undetectable flux dominates the flux error when far from
611 source. In the following, we discuss further details of the undetectable flux error. The unde-
612 tectable flux is caused by SCDs below the detection limit. Following Platt and Stutz (2008),
613 we set the detection limit as 2 times the fit error. While the exact value of the detection limit
614 might be different for different instruments and measurement conditions, we use this value to
615 derive the general dependencies of this error term and its contribution to the total flux error.

616 VCDs are sensitive to wind speeds and the dispersion (Eqs. 9 and 10), so is the undetecta-
617 ble flux. We calculate the undetectable flux and its R_{uf}^2 along wind direction (equal to along
618 the measuring distance) as shown in Figure 14 (for an emission rate of 100 g/s). As discussed,
619 the main driver of undetectable flux increasing trend along the wind direction is attributed to
620 the wind dispersion as can be seen from Figure 14. With measuring distance far away, the un-
621 detectable flux gradually dominates the flux error which can be denoted by R_{uf}^2 trend. Large
622 wind speed also results in quick dispersion thus leads more undetectable flux. The R_{uf}^2 and
623 the undetectable flux increases rapidly under the wind speed of 8 m/s than that of 1.2 m/s for
624 both NOx and SO_2.

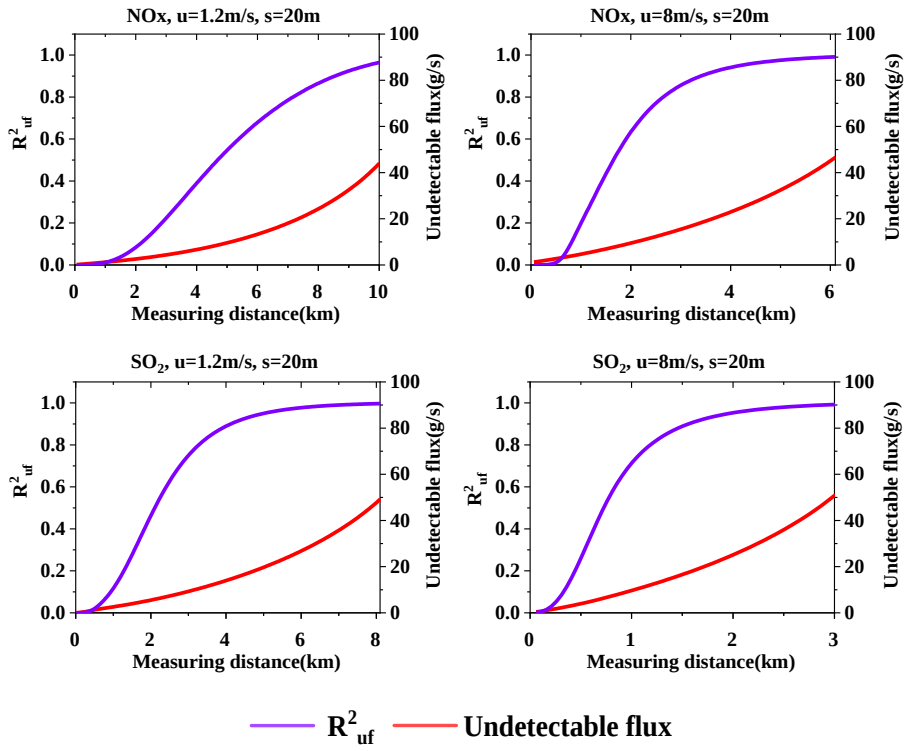

Figure 14. NOx and SO_2 absolute flux error, and the R_{uf}^2 that Undetectable SCDs result in (Q = 100 g/s).

4.6 Gas absorption cross-section error

As discussed in section 2.6, the gas absorption cross-section error contribution to SCD errors is independent of the SCD fit error. Uncertainties of the trace gas cross-sections cause systematic SCD uncertainty. We calculated R_{cro}^2 along the wind direction and the total relative errors at the speed of 1.2m/s and 8m/s, as shown in Figure 15. The R_{cro}^2 variation trend is similar to R_{uf}^2 in section 4.6 due to the relative error variation. However, maximum R_{cro}^2 has subtle difference but varies apparently along the wind direction under different wind speed, which indicates that R_{cro}^2 is not very sensitive to wind speeds but sensitive to the dispersion. From Figure 15 we see that R_{cro}^2 could approach 0.5, which means that gas cross-section error might even become the main error source. However, when R_{cro}^2 is close to 0.5, the relative errors of NOx and SO_2 are at low levels. This further suggests the trace gas cross-section error has an overall small contribution to the total flux error.

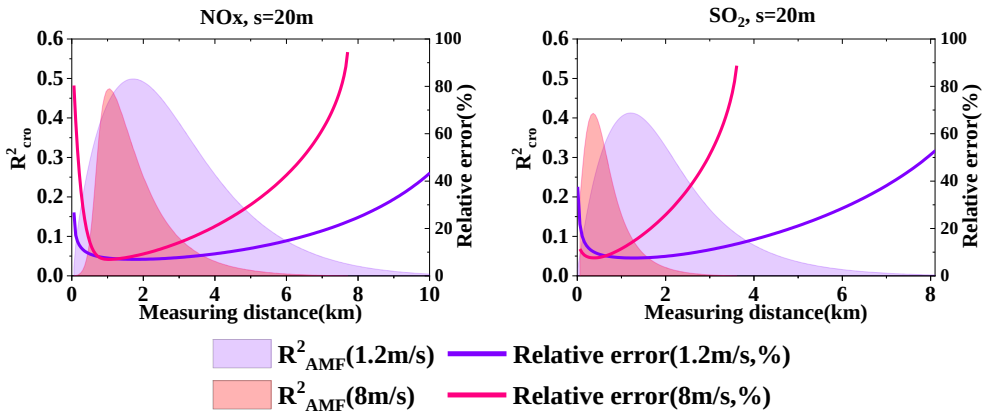

Figure 15. NOx and SO_2 R^2_{cro} of absorption cross-section error under different wind speed (Q = 100 g/s).

4.7 AMF error

AMF values depends on plume height, SZA and aerosol optical density (AOD) as shown in Figure 16. For plume heights < 50m, the AMF is around 1.03 and its error can be neglected. For plume heights ≦ 250m, the AMF error is about ±10%. Since the plume height in our study is about 250m, the contribution from the AMF error has to be taken into account.

Since VCDs are derived from SCDs by dividing the AMF, then AMF errors introduce VCD errors, which furthermore contribute to the emission flux errors. Wind speed uncertainty is the main error source when close to the source. With larger wind speed, the relative error of the wind speed becomes smaller which then also contributes less to the flux error. This indicates that the flux error that results from other error sources, such as the AMF error, have larger relative contributions under larger wind speed. Figure 17 presents R^2_{AMF} and the total relative errors for wind speeds of 1.2 m/s and 8 m/s. From Figure 17 we could see that R^2_{AMF} for SO_2 under the speed of 1.2 m/s is very small while it becomes larger at the speed of 8m/s, even near 0.5 when near the source. The NOx flux error, however, is less affected by the AMF error for $R^2_{AMF} < 0.1$.

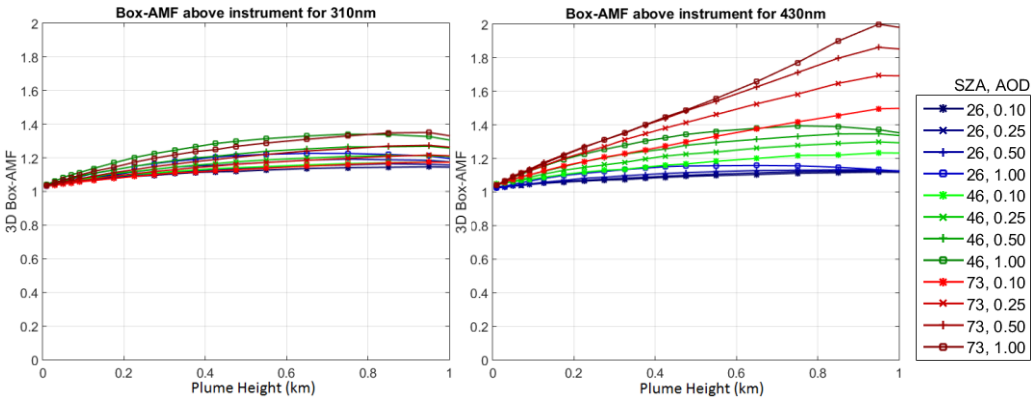

Figure 16. 3D Box-AMF dependence on plume height, SZA and aerosol optical density (AOD) for 310nm and 430nm. For the aerosols a box profile between the surface and 1km was assumed.

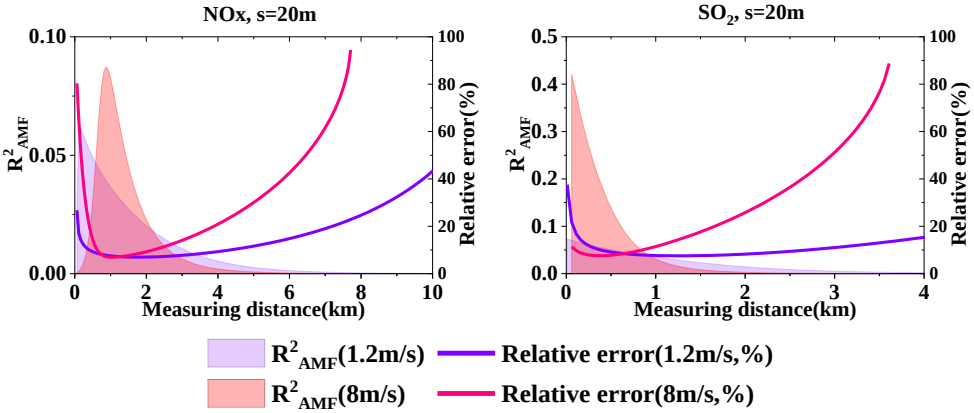

Figure 17. NOx and SO_2 total relative error, R^2_{AMF} of AMF error under different wind speed (Q = 100 g/s, s=20m).

4.8 Effect of number of measurement times

In our experiments, we only simulated a single scan of the plume by the mobile DOAS at each specific distance. In reality, we usually scan the plume cross-section several times in order to reduce the flux error. The elapsed time between two scans at the same distance from the source is then also an important parameter. The more of the elapsed time, the greater the uncertainties due to temporal variations of the flux and/or the wind fields are likely to be. Here, we assumed that the elapsed time is small and its influence can thus be neglected in our simulation. Figure 18 displays the simulation example of NOx and SO_2 flux error under different measurement times.

The error sources of the emission flux can be classified into 2 types. The first is the measurable error/uncertainty: wind speed uncertainty, AMF error and undetectable flux. The sec-

ond is: [NOx]/[NO_2] ratio correction error near the source and the gas absorption cross-section error. The flux error resulting from the first type of error source can be lowered by scanning the plume more times while the second cannot. Undetectable SCDs result in undetectable flux, and it can be reduced by more measurements times in theory. In reality, this is often not possible because it requires that all measurement conditions (e.g. the wind field or the background concentrations) stay unchanged. This means that the undetectable flux is hard to be lowered by more time scanning in the actual measurements, although it can be easily realized in theory. Therefore, in practice also the undetectable flux error belongs to the second type of errors, which cannot be reduced by multiple measurements.

According to the analysis in Section 4.3, the undetectable flux is the main error source when far from the emission source. Consequently, the flux error under different numbers of scans for both NOx and SO_2 cannot be significantly lowered when measuring far from the source (range D in Figure 18). Within the close measurement range (range C in Figure 18), the first type of error source is the predominant source of SO_2 error, and thus the flux error can be lowered by additional plume scans. For NOx, however, the [NOx]/[NO_2] ratio correction error is the main error source when very close to the emission source (range A in Figure 18), and thus the effect of additional plume scans is not evident. A little farther from the source, the first type of error source becomes the main error source (range B in Figure 18). Ultimately, the impact of additional plume scans becomes effective.

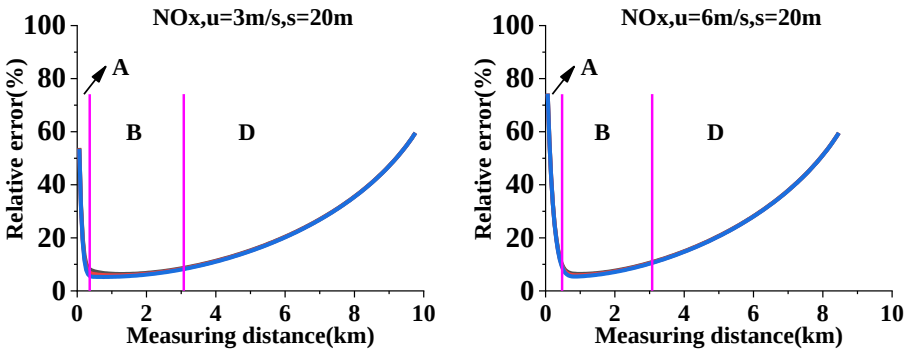

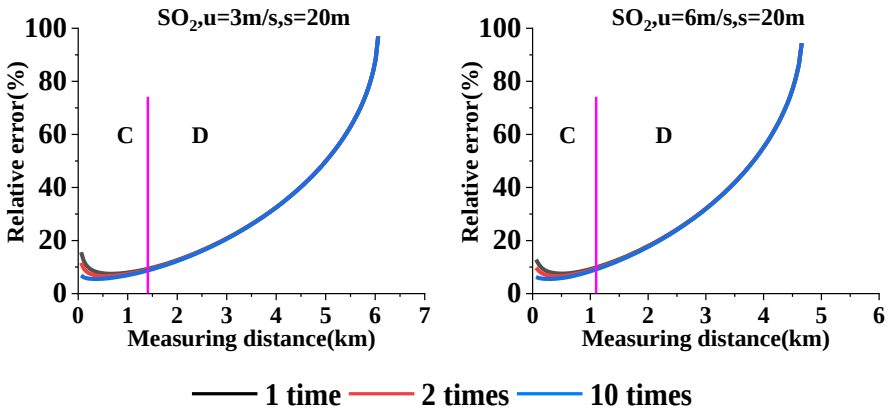

Figure 18. Emission flux error under different numbers of scans. Range A is very close to the source, range B is not too close or too far, range C is close to the source, and D is far from the source (Q = 100 g/s).

4.9 Effect of spectrometer integration times

Spectrometer noise is the main noise source of the mobile DOAS instrument (Platt and Stutz, 2008; Danckaert et al., 2015). The noise level varies under different integration times, thereby changing the fit error and detection limit, which would then affect the flux measurement error. Therefore, this section is focused on the effect of spectrometer integration times on mobile DOAS flux measurement error.

The relationships among fit error, detection limit, and noise level are (Kraus, 2006; Platt and Stutz, 2008)

$$SCD_{fit} \propto Fit_{err} \propto \sigma, \quad D_{\lim} \propto \sigma \tag{20}$$

where SCD_{fit} is the *SCD* fitting error, Fit_{err} is the residual in DOAS fitting, $D_{\lim}$ is the detection limit, and σ is the noise level. The noise level is approximately inversely proportional to the square root of the integration times.

The sampling resolution of mobile DOAS can be expressed as:

$$s = v \cdot (t_s \cdot n) = v \cdot t_{\text{int}} \tag{21}$$

where v is the car speed, t_s is a single integration time of the spectrometer, n is the spectrometer averaging times, and t_{int} is the spectrometer integration times.

According to Eq. (21), the effect of integration times can be investigated in 2 different ways: Varying the car speed and thus fixing the sampling resolution or fixing the car speed and thus

varying the sampling resolution. In this study, we simulated the integration times for $0.25\,t_{int}$, $0.5\,t_{int}$, $1\,t_{int}$, $2\,t_{int}$ and $4\,t_{int}$.

4.9.1 Prescribed sampling resolution

Since different integration times results in the car speed varying in a large range that car speed cannot be fully realized in actuality at a given sampling resolution, the sampling resolution cannot be too small. Here, we chose a 50 m sampling resolution as a case study.

Figure 19 displays the relative error under different integration times at a given sampling resolution (Q = 100 g/s). From Figure 19 we can see the relative error differences resulting from various integration times.

Since a larger integration times will directly lead to a lower detection limit and a smaller fitting error, and indirectly to a lower undetectable flux and a lower fit error, the relative error nonlinearly decreases with increasing integration times. Since the relative error differences caused by integration times become more evident when far from the source (range B in Figure 19), our analysis focused on this range. This phenomenon is due to that fact that different integration times mainly act on the fit error and the detection limit. Therefore, we separately analyzed these 2 error sources.

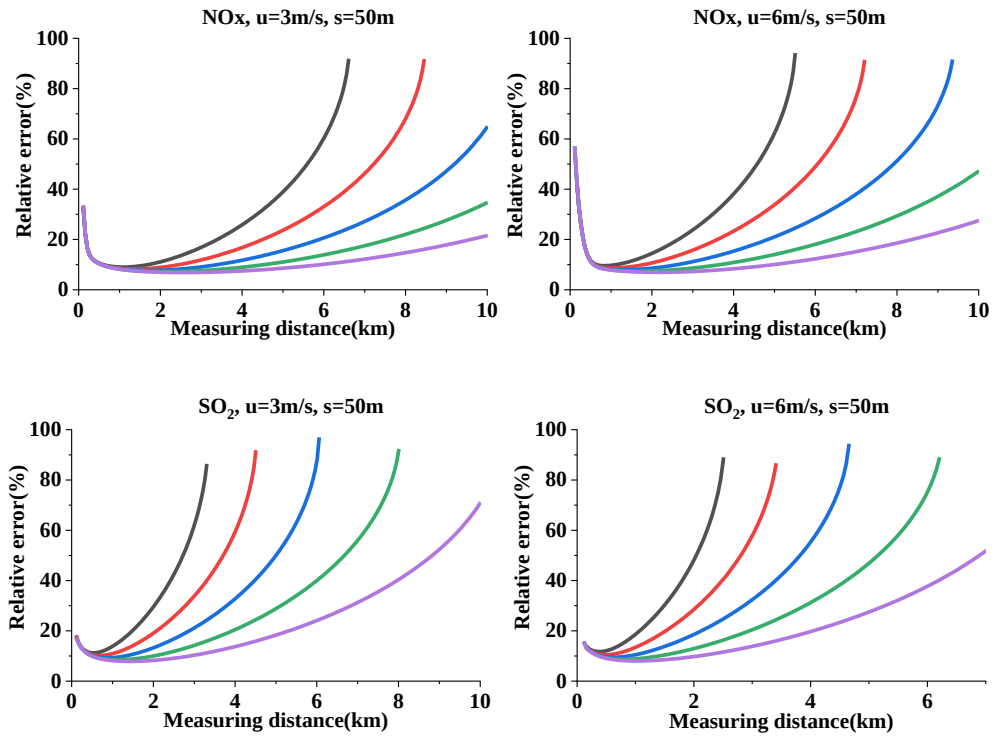

Figure 19. Relative error under different integration times at a prescribed sampling resolution (Q = 100 g/s).

We analyzed the undetectable flux differences resulting from different detection limits. Figure 20 presents the undetectable flux and its R^2 values. From the R^2 values we could infer that undetectable flux contributes most to the error when far from the source. Especially for smaller integration times, undetectable flux R^2 increases very quickly with distance. In addition, the variation trend of undetectable flux when far from the source corresponds to the relative error trend. Therefore, we infer that the relative error trend under different integration times is determined by the undetectable flux.

In brief, different integration times significantly impact the relative error at a given sampling resolution when far from the source, and these error differences are mainly attributed to the undetectable flux differences resulting from the detection limit.

.

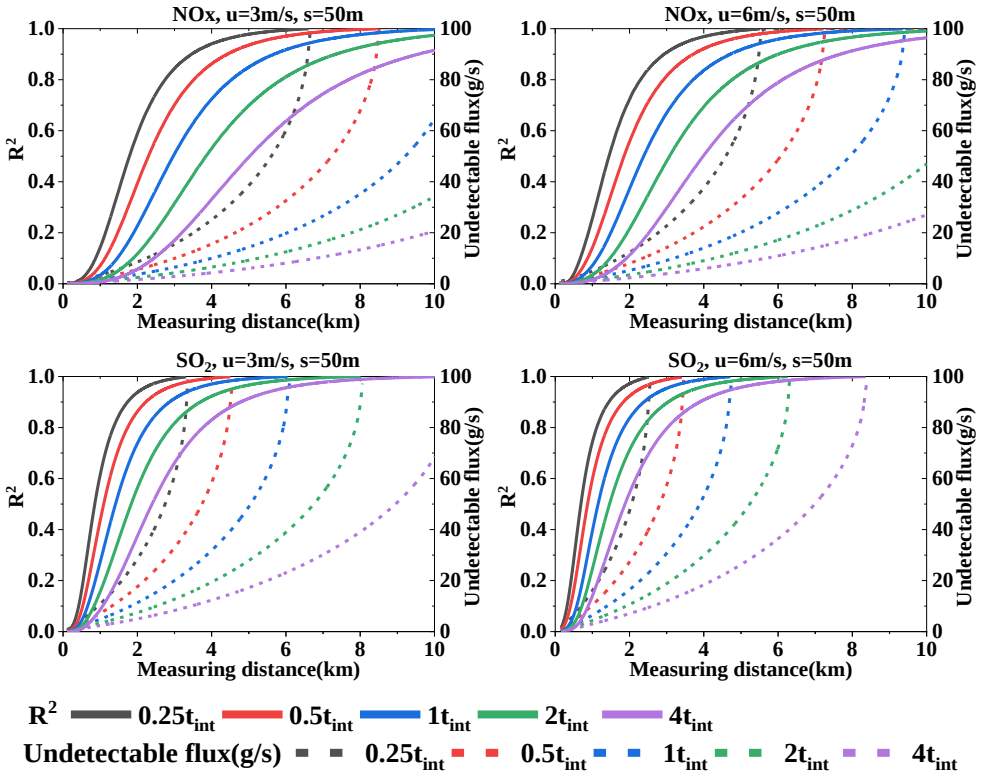

Figure 20. Undetectable flux and its R^2 values under wind speeds of 3 m/s and 6 m/s for NOx and SO_2 under different integration times. The sampling resolution is 50 m (Q = 100 g/s).

4.9.2 Prescribed car speed

When the car speed is prescribed, the sampling resolution is determined by the integration

762 times. Therefore, an effect on the error due to the sampling resolution would be introduced
763 (Section 4.1).

764 Figure 21 presents the relative error under different integration times at a given car speed. It
765 is interesting that the relative error differences caused by integration times in ranges B and D
766 (NOx) are opposite those of ranges C and D (SO_2). We have analyzed the causes of the rela-
767 tive error differences in range D, but did not analyze the causes in range B or C.

768 From Section 4.1 we know that, within the proper resolution range, the relative error in-
769 creases with increasing sampling resolution. Moreover, the sampling resolution can only af-
770 fect the first type of error source mentioned in Section 4.6, i.e., the wind speed uncertainty,
771 and AMF error. We calculated the sum of the R^2 values for the wind field uncertainty, and fit
772 error. In addition, the sum of the absolute flux errors introduced by these error sources is
773 shown in Figure 22. The R^2 values indicate that, in range B or C, these factors are the main
774 error source and thus cause the differences under different t_{int}. The flux error trends do not
775 all correspond to the relative error trend due to the undetectable flux, although it is still the
776 main error source that determines the differences in range B or C.

777 Furthermore, we can conclude that the different integration times that significantly affect
778 the relative error at a given car speed can be divided into 2 ranges: B and D for NOx, and C
779 and D for SO_2. In range B/C, the differences under different t_{int} can be attributed to the
780 sampling resolution effect. In range D, the differences under different t_{int} can be attributed
781 to the undetectable flux.

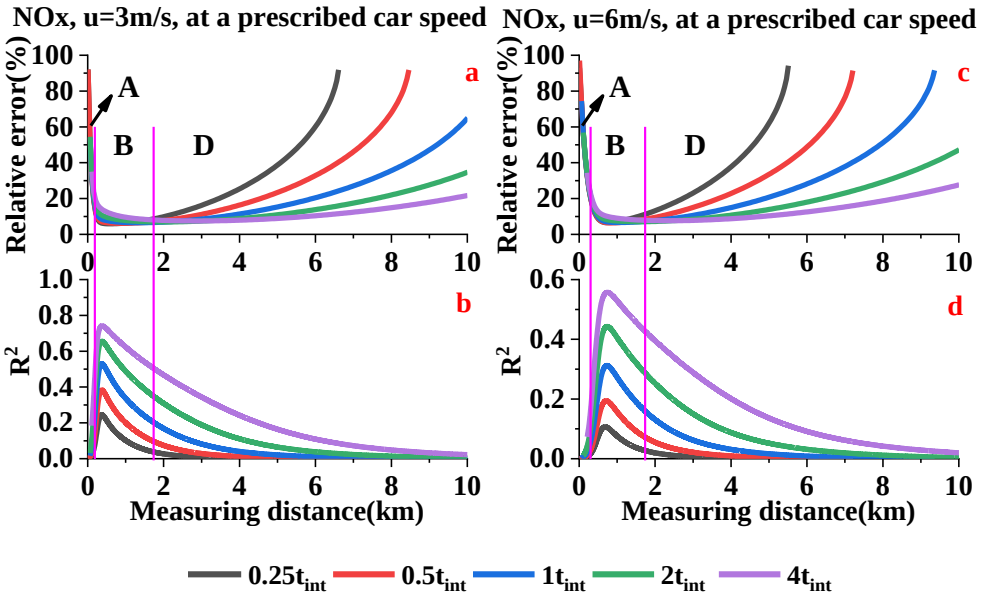

Figure 21. NOx relative errors (**a** and **c**), R^2 values introduced by the wind field uncertainty AMF error (**b** and **d**)(Q = 100 g/s).

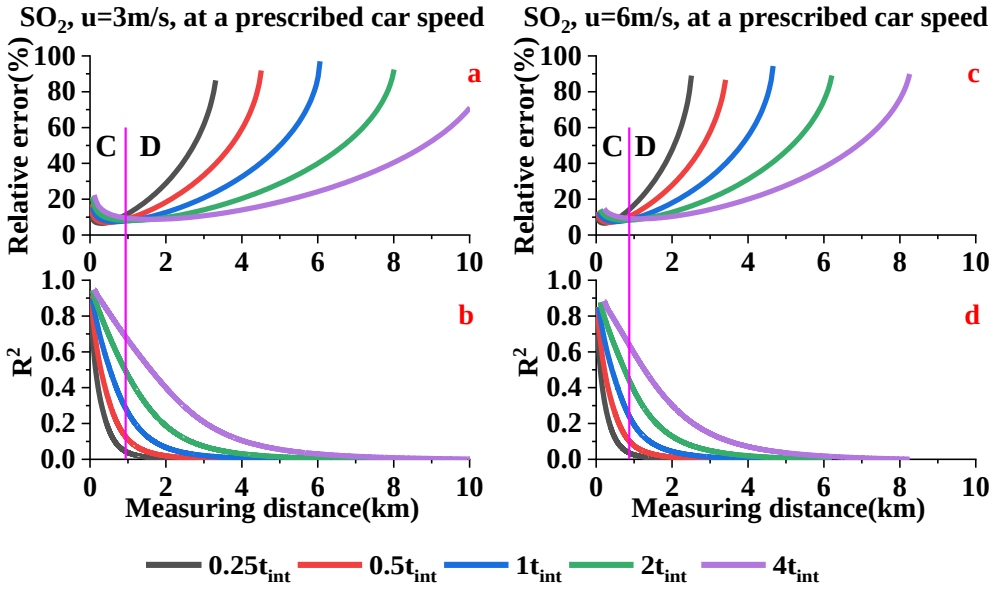

Figure 22. SO_2 relative errors (**a** and **c**), R^2 values, and flux errors introduced by the wind field uncertainty and AMF error (**b** and **d**) under wind speeds of 3 m/s and 6 m/s (Q = 100 g/s).

Different integration times result in different fit errors and different detection limits. The analysis in terms of either a given sampling resolution or a given car speed has significant implications. For example, when measuring close to the source, i.e., range B or C in Figures 21 and 22, we can fix the car speed within a proper low integration times in order to obtain a higher resolution, which indirectly results in a lower error. When measuring far from the source, proper large sampling resolutions are available since the main error source is the un-

detectable flux. This further suggests that larger integration times and higher car speeds can be applied in order to increase the efficiency of measuring flux.

4.10 Effects from other factors

Measuring emission flux is extremely complex. It is feasible to analyze the error caused by some key factors, but it is also necessary to study other factors.

4.10.1 Emission rate

Emission rate is an objective factor. The simulation results suggest that the emission rate significantly affects the relative error distribution. Therefore, disregarding the emission rate in order to analyze the error is a less rigorous approach.

From Eqs. (9), (10), and (11) we know that VCD(x,y) is proportional to the emission rate, which means that lower emission rates generate lower VCD(x,y), leading to a reduction of the measurable plume width with SCDs above the detection limit. Ultimately, this results in larger emission flux errors at the same distance when the emission rate is low, even if there is no proper resolution to measure. In order to achieve a low emission flux error, emission rates that are too low are not recommended. We cannot provide a precise lower limit for the emission rate, but can propose a range of values. From the figures in the Appendix, we can see that the red areas (indicating large errors) cover nearly all of the figure when the NOx emission rate is < 30 g/s and the SO_2 emission rate is < 50 g/s. Therefore, emission rates < 30 g/s for NOx and < 50 g/s for SO_2 are not recommended in mobile DOAS measurements.

4.10.2 Different source heights

The mobile DOAS height, which is approximately 2 m from the ground to the telescope, is usually negligible in actual measurements. When the source is not very high, however, more gas will descend to the ground under the mobile DOAS telescope, where it cannot be measured. Here, we simulated the emission source at heights of 10 m, 20 m, 50 m, 100 m, and 200 m. Since lower wind speeds will lead to gas quickly descending to the ground, we simulated a low wind speed of 3 m/s. The emission rate was set to 100 g/s.

The lower the source height, the more gas will descend to the ground, resulting in changes to the undetectable flux. Figure 23 displays the undetectable flux of NOx and SO_2 for the

wind speed of 3 m/s. From this figure we can see that obvious variations occur in the NOx and SO_2 undetectable flux when close to the source. The undetectable flux variation may impact the flux relative error.

Figure 24 presents the flux relative error at different heights. These results show that the relative errors of NOx and SO_2 exhibit little variation. This is because, compared to the flux error resulting from other main error sources, the undetectable flux variation with height is negligible.

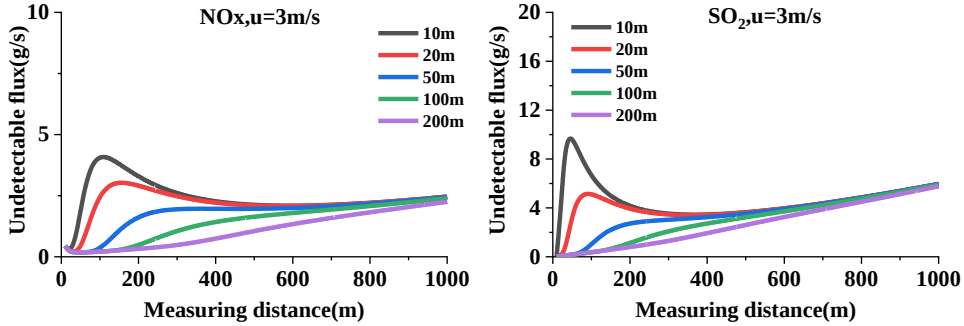

Figure 23. NOx and SO_2 undetectable flux values at different source heights (Q = 100 g/s, u = 3 m/s).

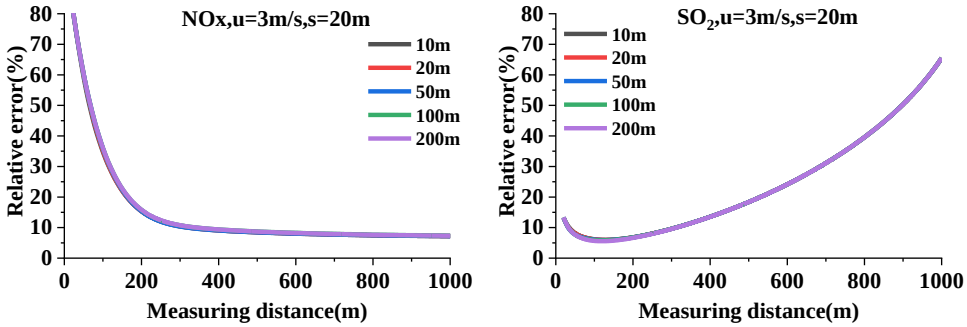

Figure 24. NOx and SO_2 flux relative errors at different source heights (Q = 100 g/s, u = 3 m/s, *s* = 20 m).

4.10.3 Uncertainties of the Gaussian dispersion model

The Gaussian dispersion model was assumed in the forward model during our discussion of the emission flux error budget. The dispersion in actual measurements, however, depends on meteorological conditions and surrounding terrain. Also a non-Gaussian behavior of the plume and vertical wind shear might contribute to the total flux error. Thus, the results of this study should be seen as a lower limit of the total flux errors. In some cases, for NO_2, also the stratospheric absorption might become important. However, this might only happen for very long measurement durations or for measurements at high SZA. Differences in the Gaussian dispersion model from reality could have resulted in a bias of the error budget presented in

this study from reality. The investigation of the detailed of the dispersion model is outside the scope of this investigation.

5 Conclusions

In this study, we used a Gaussian dispersion model to quantify the NOx and SO_2 point source emission flux errors of mobile DOAS.

We first established a forward model for the simulation.

In the forward model, we modified the Gaussian dispersion model in order to make it appropriate for the DOAS technique, i.e., the SO_2 and NOx VCD dispersion model. The NOx VCD dispersion model also took NOx atmospheric chemical reactions into consideration.

Second, we analyzed the simulation data, reaching the following conclusions:

(1) The impact of sampling resolution on emission flux error is noticeable. Smaller resolution can lower the flux error. In terms of measurement efficiency, the sampling resolution should be moderate. Therefore, we recommended the proper sampling resolution to range from 5–50 m. Larger resolutions could also be applied, but > 100 m is not recommended.

(2) Measuring distance significantly affects the flux measurement error. When far from the source, undetectable flux from the wind dispersion effect, which results in large errors, will be noticeable. When close to the emission source, a low number of sampling data leads to large flux errors. The proper measuring distance is not too far or too close to the source. Due to the complex situation, the proper distance is difficult to quantify. It should be noted that undetectable flux is the error source which was not considered in (Johansson et al., 2008, 2009; Rivera et al., 2009, 2012; Ibrahim et al., 2010; Shaiganfar et al., 2011, 2017; Berg, et al.,2012; Walter, 2012 et al.; Wu et al., 2013, 2017; Frins et al., 2014; Merlaud et al., 2018).

(3) The wind field influence could be classified into 2 parts: uncertainty and dispersion. Dispersion is more evident when far from the emission source; thus, undetectable flux is the main error source for both SO_2 and NOx. When measuring close to the emission source, wind field uncertainty is the main error source of SO_2 flux measurements, but not of NOx. For higher wind speeds, the dispersion effect is more distinct, thereby directly leading to more undetectable flux. We recommended a wind speed of 1–4 m/s for accurate mobile DOAS

873 measurements.

874 **(4)** NO converts to NO_2 upon exhaust from a stack and reaches the NOx steady-state within
875 a few minutes. During this time period the [NOx]/[NO_2] ratio decreases continuously with
876 distance, resulting in a flux error due to [NOx]/[NO_2] ratio correction. Our simulation indi-
877 cates that [NOx]/[NO_2] ratio correction is the main error source when measuring very close to
878 the emission source. To minimize the large [NOx]/[NO_2] ratio correction error, we recom-
879 mended $r_{NO2} = 0.05 r_{\max}$ as the NOx steady-state. Therefore, the proper starting measurement
880 distance for NOx could be determined, which we displayed in Figure 13.

881 **(5)** The undetectable flux is sensitive to wind speeds and wind dispersion.

882 **(6)** The AMF error is not the main error source for NOx; for SO_2 it can only become im-
883 portant for measurements close to the source and for high wind speeds.

884 **(7)** The gas absorption cross-section error might become the main error source when at low
885 levels but in such conditions the absolute flux error is rather small.

886 **(8)** Repeating the measurements several times can only affect the measurable error source,
887 and do not affect the unmeasurable. This causes the SO_2 flux error to decrease when not very
888 far from the emission source. As for NOx, increasing the number of measurement times could
889 become effective when not very close to the source but not too far away.

890 **(9)** Different integration times result in different fit errors and detection limits. For a pre-
891 scribed sampling resolution, relative error differences under different integration times are
892 attributed to undetectable flux differences caused by the detection limit, especially for distant
893 measurements. For a prescribed car speed, the sampling resolution effect is introduced. When
894 measuring not very far from the emission source, the relative error differences are attributed
895 to the sampling resolution effect from the first type of error source. Far from the source, the
896 detection limit applies.

897 **(10)** Other studies have indicated that emission rates < 30 g/s for NOx and < 50 g/s for SO_2
898 are not recommended in mobile DOAS measurements. The source height exerts an impact on
899 the undetectable flux, but has little impact on the total error.

900 The advantage of the method put forth in this study is that many scenarios can be simulated.

This simulation method was able to examine the error sources and influence factors affecting flux error in more detail. Also important is that the [NOx]/[NO_2] ratio correction effect of flux measurement was clarified.

Data availability. The data used in this analysis are available from the authors upon request.

Author contributions. Ang Li, Thomas Wagner and Yeyuan Huang developed the simulation method. Yeyuan Huang, Yang Wang and Zhaokun Hu designed the forward model. Hongmei Ren and Bing Dang processed the wind data. Julia Remmers performed the AMF simulation. Pinhua Xie, Thomas Wagner, Jin Xu and Xiaoyi Fang supervised this study. Yeyuan Huang analyzed the data and wrote the paper. Yang Wang revised this paper preliminarily.

Competing interests. The authors declare that they have no competing interests.

Acknowledgements. This work was supported by National Natural Science Foundation of China (grant nos. 41775029, 91644110 and 41530644), National Key Research and Development Project of China 2018YFC0213201and 2017YFC0209902, Science and Technology Commission Shanghai Municipality Research Project 17DZ1203102.

References

Alicke, B., Platt, U., Stutz, J.: Impact of nitrous acid photolysis on the total hydroxyl radical budget during the Limitation of Oxidant Production/Pianura Padana Produzione di Ozono study in Milan, J. Geophys. Res., 107, NO. D22, 8196, doi:10.1029/2000JD000075, 2002.

Arystanbekova, N.Kh.: Application of Gaussian plume models for air pollution simulation at instantaneous emissions. Mathematics and Computers in Simulation, 67, 4-5. https://doi.org/10.1016/j.matcom.2004.06.023, 2004.

Bobrowski, N., Honninger, G., Galle, B., and Platt U.: Detection of bromine monoxide in a volcanic plume, Nature, 423, 273–276,2003.

Beirle, S., Hörmann, C., Penning de Vries, M., Dörner, S., Kern, C., and Wagner, T.: Estimat-

ing the volcanic emission rate and atmospheric lifetime of SO_2 from space: a case study for Kīlauea volcano, Hawai`i, Atmos. Chem. Phys., 14, 8309–8322, https://doi.org/10.5194/acp-14-8309-2014, 2014.

Beirle, S., Platt, U., Wenig, M., and Wagner, T.: Weekly cycle of NO_2 by GOME measurements: a signature of anthropogenic sources, Atmos. Chem. Phys., 3, 2225–2232, https://doi.org/10.5194/acp-3-2225-2003, 2003.

Berg, N., Mellqvist, J., Jalkanen, J.-P., and Balzani, J.: Ship emissions of SO_2 and NO_2: DOAS measurements from airborne platforms, Atmos. Meas. Tech., 5, 1085–1098, https://doi.org/10.5194/amt-5-1085-2012, 2012.

Danckaert, T., Fayt, C., van Roozendael, M., de Smedt, I., Letocart, V., Merlaud, A., and Pinardi, G.: QDOAS Software user manual, available at: http://uv-vis.aeronomie.be/software/QDOAS/QDOAS_manual.pdf (last access: 9 September 2016), 2015.

Davis, Z. Y. W., Baray, S., McLinden, C. A., Khanbabakhani, A., Fujs, W., Csukat, C., Debosz, J. and McLaren, R.: Estimation of NOx and SO_2 emissions from Sarnia, Ontario, using a mobile MAX-DOAS (Multi-AXis Differential Optical Absorption Spectroscopy) and a NOx analyzer, Atmos. Chem. Phys., 19, 13871–13889, https://doi.org/10.5194/acp-19-13871-2019, 2019.

de Visscher, Alex.: AIR DISPERSION MODELING Foundations and Applications, ISBN 978-1-118-07859-4, Wiley, New York, 2014.

Deutschmann, T.; Beirle, S.; Frieß, U.; Grzegorski, M.; Kern, C.,Kritten, L.; Platt, U.; Prados-Roman, C.; Pukite, J.; Wagner, T.; Werner, B.; Pfeilsticker, K., The Monte Carlo atmospheric radiative transfer model McArtim: introduction and validation of Jacobians and 3-D features, J. Quant. Spectrosc. Ra., 112, 1119–1137, 2011, https://doi.org/10.1016/j.jqsrt.2010.12.009.

Ding, J., van der A, R. J., Mijling, B., Levelt, P. F., and Hao, N.: NOx emission estimates during the 2014 Youth Olympic Games in Nanjing, Atmos. Chem. Phys., 15, 9399–9412, https://doi.org/10.5194/acp-15-9399-2015, 2015.

Deutschmann, T.; Beirle, S.; Frieß, U.; Grzegorski, M.; Kern, C.,Kritten, L.; Platt, U.; Prados-Roman, C.; Pukite, J.; Wagner, T.; Werner, B.; Pfeilsticker, K., The Monte Carlo atmospheric radiative transfer model McArtim: introduction and validation of Jacobians and 3-D features, J. Quant. Spectrosc. Ra., 2011, 112, 1119–1137.

Edmonds, M., Herd, R. A., Galle, B., and Oppenheimer, C. M.: Automated high-time resolution measurements of SO_2 flux at Soufrière Hills Volcano, Montserrat, B. Volcanol., 65, 578–586, 2003.

Frins, E., Bobrowski, N., Osorio, M., Casaballe, N., Belsterli, G., Wagner, T. and Platt, U.: Scanning and mobile Multi-Axis DOAS measurements of SO_2 and NO_2 emissions from an electric power plant in Montevideo, Uruguay. Atmos. Environ., 98, 347–356. https://doi.org/10.1016/j.atmosenv.2014.03.069, 2014.

Galle, B., Oppenheimer, C., Geyer, A., McGonigle, A.J.S., Edmonds, M. and Horrocks, L.: A miniaturized ultraviolet spectrometer for remote sensing of SO_2 fluxes: A new tool for volcano surveillance. J. Volcanol. Geother. Res., 119, 241–254, 2003.

Hönninger, G., von Friedeburg, C., and Platt, U.: Multi axis differential optical absorption spectroscopy (MAX-DOAS), Atmos. Chem. Phys., 4, 231–254, https://doi.org/10.5194/acp-4-231-2004, 2004.

Ibrahim, O., Shaiganfar, R., Sinreich, R., Stein, T., Platt, U., and Wagner, T.: Car MAX-DOAS measurements around entire cities: quantification of NOx emissions from the cities of Mannheim and Ludwigshafen (Germany), Atmos. Meas. Tech., 3, 709–721, https://doi.org/10.5194/amt-3-709-2010, 2010.

Jin, J., Ma, J., Lin, W., Zhao, H., Shaiganfar, R., Beirle, S., and Wagner, T.: MAX-DOAS measurements and satellite validation of tropospheric NO_2 and SO_2 vertical column densities at a rural site of North China, Atmos. Environ., 133, 12–25, https://doi.org/10.1016/j.atmosenv.2016.03.031, 2016.

Johansson, M., Galle, B., Yu, T., Tang, L., Chen, D., Li, H., Li, J., Zhang, Y.: Quantification of total emission of air pollutants from Beijing using mobile mini-DOAS. Atmos. Environ., 42,6926–6933. https://doi.org/10.1016/j.atmosenv.2008.05.025, 2008.

985 Johansson, M., Rivera, C., de Foy, B., Lei, W., Song, J., Zhang, Y., Galle, B., and Molina, L.:
986 Mobile mini-DOAS measurement of the outflow of NO_2 and HCHO from Mexico City,
987 Atmos. Chem. Phys., 9, 5647–5653, https://doi.org/10.5194/acp-9-5647-2009, 2009.
988 Kraus, S.: DOASIS, A Framework Design for DOAS, PhD thesis, University of Mannheim
989 (http://hci.iwr.uni-heidelberg.de/publications/dip/2006/Kraus PhD2006.pdf), 2006.
990 Lushi, E., Stockie, J. M.: An inverse Gaussian plume approach for estimating atmospheric
991 pollutant emissions from multiple point sources. Atmos. Environ., 44, 1097-1107.
992 https://doi.org/10.1016/j.atmosenv.2009.11.039, 2009.
993 Merlaud, A., Tack, F., Constantin, D., Georgescu, L., Maes, J., Fayt, C., Mingireanu, F.,
994 Schuettemeyer, D., Meier, A. C., Schönardt, A., Ruhtz, T., Bellegante, L., Nicolae, D., Den
995 Hoed, M., Allaart, M., and Van Roozendael, M.: The Small Whiskbroom Imager for at-
996 mospheric compositioN monitorinG (SWING) and its operations from an unmanned aerial
997 vehicle (UAV) during the AROMAT campaign, Atmos. Meas. Tech., 11, 551–567,
998 https://doi.org/10.5194/amt-11-551-2018, 2018.
999 Platt, U. and Stutz, J.: Differential Optical Absorption Spectroscopy (DOAS), Principles and
1000 Applications, ISBN 978-3-540-21193-8, Springer, Berlin-Heidelberg, 2008.
1001 Richter, A., Burrows, J. P., Nüß, H., Granier, C., and Niemeier, U.: Increase in tropospheric
1002 nitrogen dioxide over China observed from space, Nature, 437, 129–132, 2005.
1003 Rivera, C., Sosa, G., Wöhrnschimmel, H., de Foy, B., Johansson, M., and Galle, B.: Tula in-
1004 dustrial complex (Mexico) emissions of SO_2 and NO_2 during the MCMA 2006 field cam-
1005 paign using a mobile mini-DOAS system, Atmos. Chem. Phys., 9, 6351–6361,
1006 https://doi.org/10.5194/acp-9-6351-2009, 2009.
1007 Seinfeld, J. H. and Pandis, S. N.: Atmospheric Chemistry and Physics – From Air Pollution to
1008 Climate Change, John Wiley, New York, 1998.
1009 Shaiganfar, R., Beirle, S., Sharma, M., Chauhan, A., Singh, R. P., and Wagner, T.: Estimation
1010 of NOx emissions from Delhi using Car MAX-DOAS observations and comparison with
1011 OMI satellite data, Atmos. Chem. Phys., 11, 10871–10887,
1012 https://doi.org/10.5194/acp-11-10871-2011, 2011.

Shaiganfar, R., Beirle, S., Denier van der Gon, H., Jonkers, S., Kuenen, J., Petetin, H., Zhang, Q., Beekmann, M., and Wagner, T.: Estimation of the Paris NOx emissions from mobile MAX-DOAS observations and CHIMERE model simulations during the MEGAPOLI campaign using the closed integral method, Atmos. Chem. Phys., 17, 7853–7890, https://doi.org/10.5194/acp-17-7853-2017, 2017.

Spicer, C. W.: Nitrogen Oxide Reactions in the Urban Plume of Boston. Science, 215, 1095–1097. http://www.sciencemag.org/cgi/doi/10.1126/science.215.4536.1095, 1982.

Theys, N., Van Roozendael, M., Hendrick, F., Fayt, C., Hermans, C., Baray, J. L., Goutail, F., Pommereau, J. P., De Maziere, M.: Retrieval of stratospheric and tropospheric BrO columns from multi-axis DOAS measurements at Reunion Island (21 ° S, 56 ° E). Atmos. Chem. Phys., 18, 4733-4749, https://doi.org/10.5194/acp-7-4733-2007, 2007.

Vandaele, A. C., Simon P. C., Guilmot, J. M. Carleer, M., Colin, R.: SO2 absorption cross section measurement in the UV using a Fourier transform spectrometer, J. Geophys. Res., 99, D12, https://doi.org/10.1029/94JD02187, 1994.

Vandaele, A.C., Hermans, C., Simon, P.C., Carleer, M., Colin, R., Fally, S., Mérienne, M.F., Jenouvrier, A., Coquart, B.: Measurements of the NO2 absorption cross-section from 42 000 cm−1 to 10000 cm−1 (238–1000 nm) at 220 K and 294 K, J. Quanr. .Specrrosc. Radior. Transfer, 59,171-184, DOI: 10.1016/S0022-4073(97)00168-4, 1998.

Wagner, T., Dix B., Friedeburg, C. v., Frieß, U., Sanghavi, S., Sinreich, R., and Platt, U.: MAX-DOAS O_4 measurements –a new technique to derive information on atmospheric aerosols -Principles and information content, J. Geophys. Res., 109, D22205, https://doi.org/10.1029/2004JD004904, 2004.

Wagner, T., Ibrahim, O., Shaiganfar, R., and Platt, U.: Mobile MAX-DOAS observations of tropospheric trace gases, Atmos. Meas. Tech., 3, 129–140, https://doi.org/10.5194/amt-3-129-2010, 2010.

Wagner, T., Beirle, S., Brauers, T., Deutschmann, T., Frieß, U., Hak, C., Halla, J. D., Heue, K. P., Junkermann, W., Li, X., Platt, U., and Pundt-Gruber, I.: Inversion of tropospheric profiles of aerosol extinction and HCHO and NO_2 mixing ratios from MAX-DOAS observa-

tions in Milano during the summer of 2003 and comparison with independent data sets, Atmos. Meas. Tech., 4, 2685–2715, https://doi.org/10.5194/amt-4-2685-2011, 2011.

Walter, D., Heue, K. P., Rauthe‐Schöch, A., Brenninkmeijer, C. A. M., Lamsal,L. N., Krotkov, N. A. Platt, U.: Flux calculation using CARIBIC DOAS aircraft measurements: SO_2 emission of Norilsk, J. Geophys. Res., 117, D11305, https://doi.org/10.1029/2011JD017335, 2012.

Wang, T., Hendrick, F., Wang, P., Tang, G., Clémer, K., Yu,H., , Fayt C., Hermans, C., Gielen, C., Müller, J.-F., Pinardi, G.,Theys, N., Brenot, H., Roozendael, M. Van.: Evaluation of tropospheric SO2 retrieved from MAX-DOAS measurements in Xianghe, China, Atmos. Chem. Phys., 14, 11149–11164, doi:10.5194/acp-14-11149-2014, 2014.

Wu, F. C., Xie, P. H., Li, A., Chan, K. L., Hartl, A., Wang, Y., Si, F. Q., Zeng, Y., Qin, M., Xu, J., Liu, J. G., Liu, W. Q., and Wenig, M.: Observations of SO_2 and NO_2 by mobile DOAS in the Guangzhou eastern area during the Asian Games 2010, Atmos. Meas. Tech., 6, 2277–2292, https://doi.org/10.5194/amt-6-2277-2013, 2013.

Wu, F., Xie, P., Li, A., Mou, F., Chen, H., Zhu, Y., Zhu, T., Liu, J., and Liu, W.: Investigations of temporal and spatial distribution of precursors SO_2 and NO_2 vertical columns in the North China Plain using mobile DOAS, Atmos. Chem. Phys., 18, 1535–1554, https://doi.org/10.5194/acp-18-1535-2018, 2018.

Zhang, H.X., Liu, C., Hu Q.H., Cai, Z.N., Su W.J., Xia, C.Z., Zhu Y.Z., Wang, S.W., Liu J.G.: Satellite UV-Vis spectroscopy: implications for air quality trends and their driving forces in China during 2005–2017. Light Sci. Appl., 8, 100 (2019), https://doi.org/10.1038/s41377-019-0210-6, 2019.

Zhang, H.X., Liu, C., Chan, K.L., Hu, Q.H., Liu, H.R., Li, B., Xing, C.Z., Tan, W., Zhou, H.J., Si, F.Q., Liu, J.G.: First observation of tropospheric nitrogen dioxide from the Environmental Trace Gases Monitoring Instrument onboard the GaoFen-5 satellite. Light Sci. Appl., 9, 66(2020), https://doi.org/10.1038/s41377-020-0306-z, 2020.

Appendix

1. NOx simulation results (relative error)

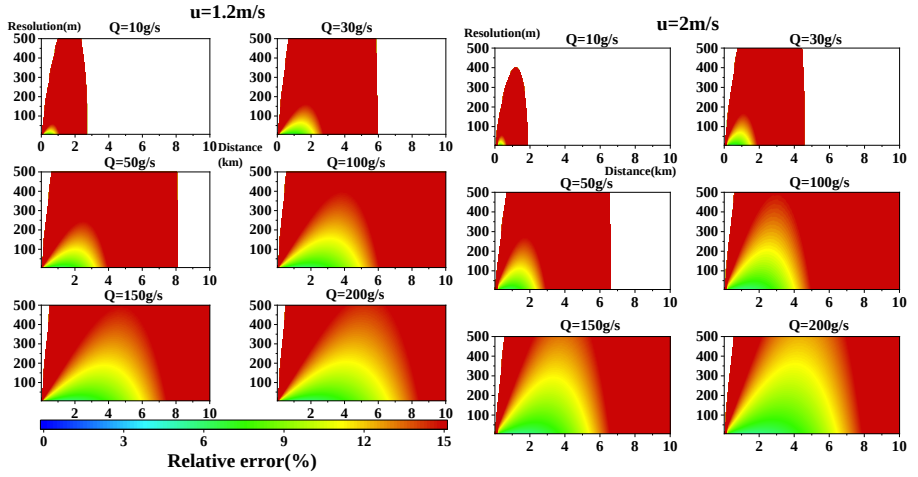

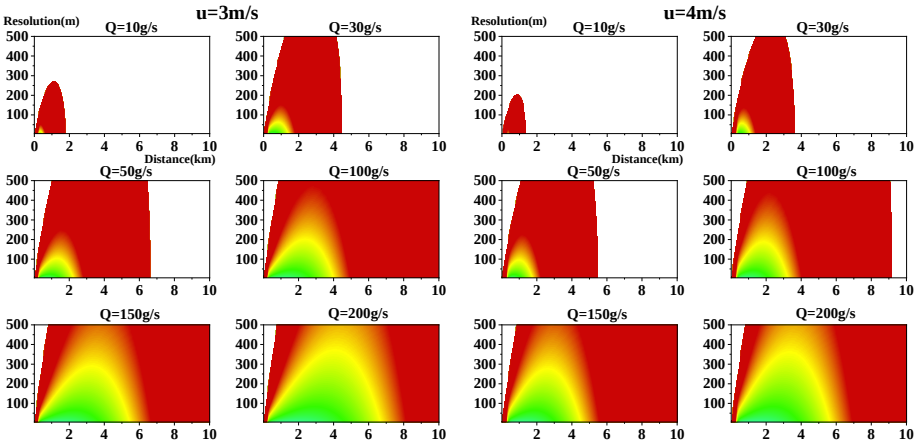

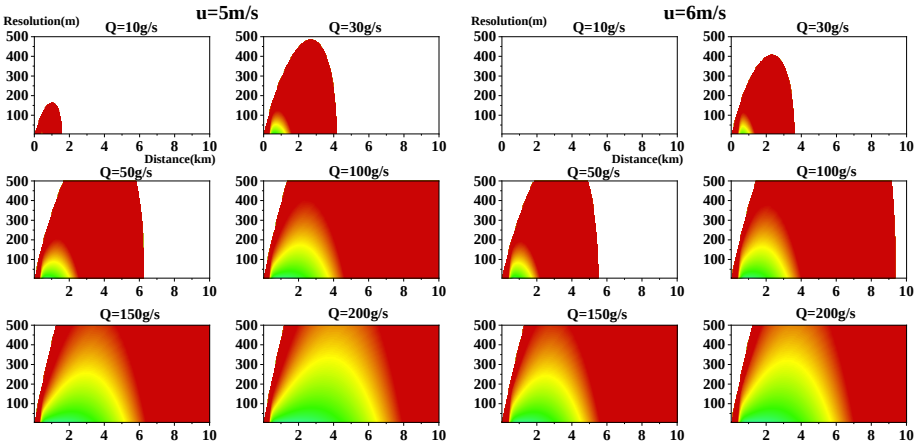

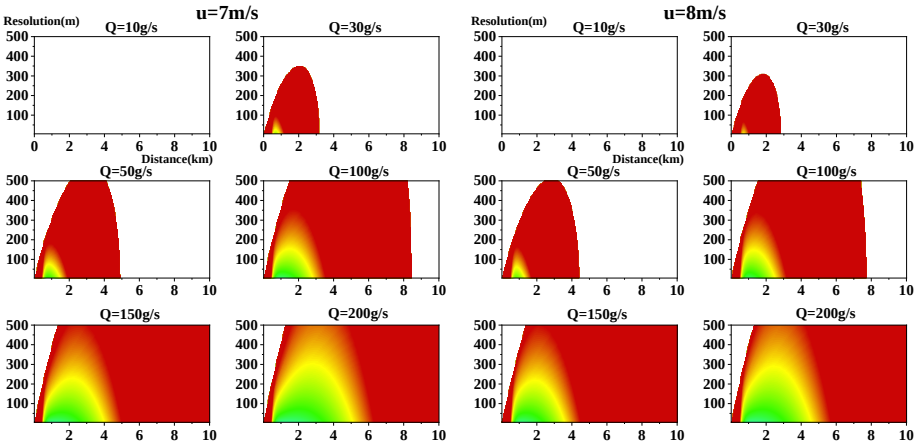

Figure 25. Relative errors (using Eq. 17) of NOx as a function of the measurement distance from the source (*x*-axis) and the sampling resolution (*y*-axis). The different subfigures show the results for different wind speeds and different emission rates. The color map indicates the relative errors.

2. SO_2 simulation results (relative error)

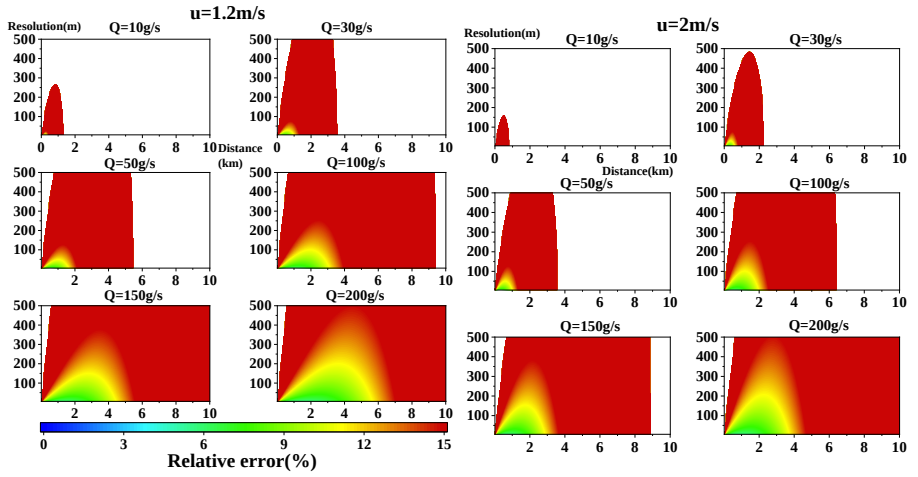

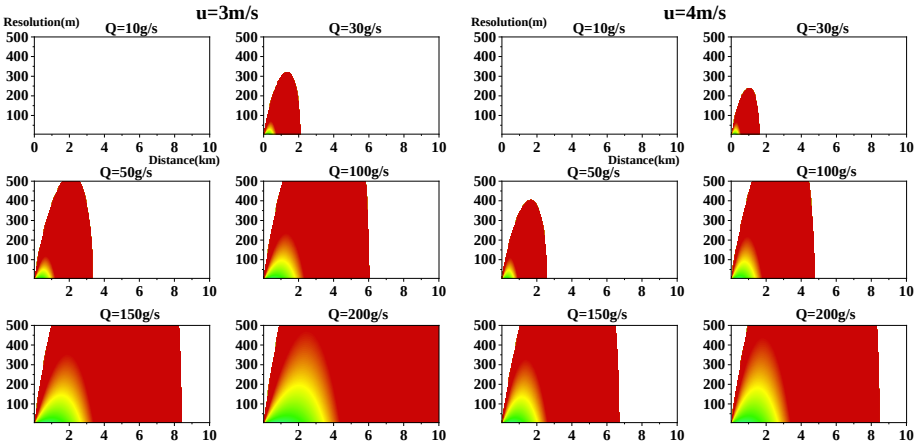

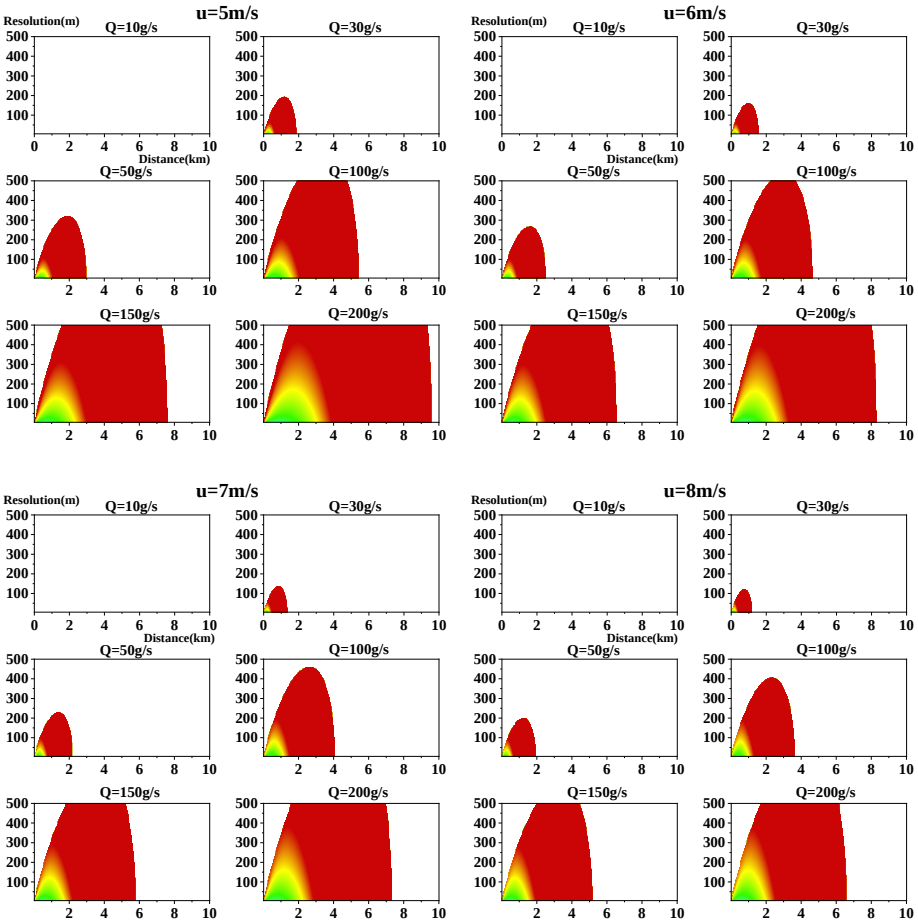

Figure 26. Relative error (using Eq. 16) of the distribution of SO_2 for different wind fields of different emission rates. The unit of all abscissas is the measurement distance from the source (km), while that of the ordinate is the sampling resolution (m). The color map indicates the relative errors.